HHS Public Access

Author manuscript

Cell Rep. Author manuscript; available in PMC 2021 October 21.

Published in final edited form as:

Cell Rep. 2021 October 05; 37(1): 109786. doi:10.1016/j.celrep.2021.109786.

β-Amyloid disruption of LTP/LTD balance is mediated by AKAP150-anchored PKA and Calcineurin regulation of Ca^{2+}-permeable AMPA receptors

Jennifer L. Sanderson[1], **Ronald K. Freund**[1], **Jessica A. Gorski**[1,4], **Mark L. Dell'Acqua**[1,2,3,5,*]

[1]Department of Pharmacology, University of Colorado School of Medicine, Anschutz Medical Campus, Aurora, CO 80045, USA

[2]University of Colorado Alzheimer's and Cognition Center, Anschutz Medical Campus, Aurora, CO 80045, USA

[3]Linda Crnic Institute for Down Syndrome, Anschutz Medical Campus, Aurora, CO 80045, USA

[4]Present address: Health Professions Residential Academic Program, University of Colorado Boulder, Boulder, CO 803098, USA

[5]Lead contact

SUMMARY

Regulated insertion and removal of postsynaptic AMPA glutamate receptors (AMPARs) mediates hippocampal long-term potentiation (LTP) and long-term depression (LTD) synaptic plasticity underlying learning and memory. In Alzheimer's disease β-amyloid (Aβ) oligomers may impair learning and memory by altering AMPAR trafficking and LTP/LTD balance. Importantly, Ca^{2+}-permeable AMPARs (CP-AMPARs) assembled from GluA1 subunits are excluded from hippocampal synapses basally but can be recruited rapidly during LTP and LTD to modify synaptic strength and signaling. By employing mouse knockin mutations that disrupt anchoring of the kinase PKA or phosphatase Calcineurin (CaN) to the postsynaptic scaffold protein AKAP150, we find that local AKAP-PKA signaling is required for CP-AMPAR recruitment, which can facilitate LTP but also, paradoxically, prime synapses for Aβ impairment of LTP mediated by local AKAP-CaN LTD signaling that promotes subsequent CP-AMPAR removal. These findings highlight the importance of PKA/CaN signaling balance and CP-AMPARs in normal plasticity and aberrant plasticity linked to disease.

Graphical Abstract

*Correspondence: mark.dellacqua@cuanschutz.edu.

AUTHOR CONTRIBUTIONS

Conceptualization, M.L.D., J.L.S., and R.K.F.; methodology, J.L.S., R.K.F., and J.A.G.; formal analysis and investigation: M.L.D., J.L.S., R.K.F., and J.A.G.; resources, M.L.D.; writing – original draft, M.L.D; writing – review & editing, M.L.D., J.L.S., R.K.F., and J.A.G.; supervision, M.L.D.; funding acquisition, M.L.D.

SUPPLEMENTAL INFORMATION

Supplemental information can be found online at https://doi.org/10.1016/j.celrep.2021.109786.

DECLARATION OF INTERESTS

The authors declare no competing interests.

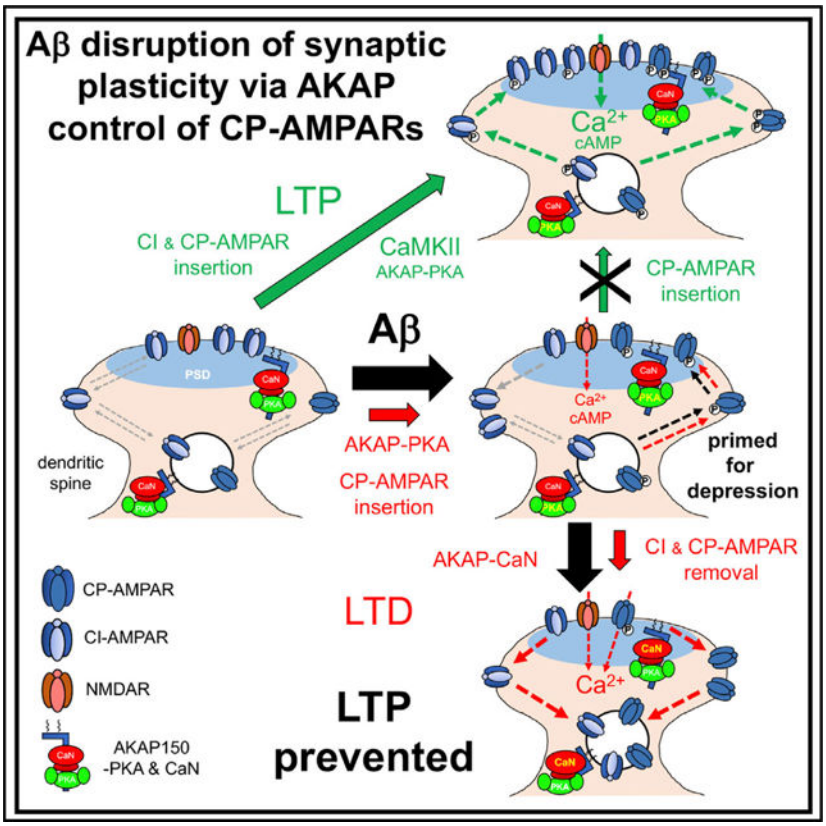

In brief

In Alzheimer's disease, Aβ oligomers disrupt hippocampal neuronal plasticity and cognition. Sanderson et al. show how the postsynaptic scaffold protein AKAP150 coordinates PKA and Calcineurin regulation of Ca^{2+}-permeable AMPA-type glutamate receptors to mediate disruption of synaptic plasticity by Aβ oligomers.

INTRODUCTION

Learning and memory require synaptic plasticity mediated by NMDA (NMDARs) and AMPA glutamate receptors (AMPARs) that includes long-term potentiation (LTP)/long-term depression (LTD) (Collingridge et al., 2010; Diering and Huganir, 2018; Huganir and Nicoll, 2013), which rapidly increase/decrease synaptic strength in response to acute stimulation, respectively, and homeostatic plasticity, which gradually adjusts synaptic strength in response to chronic activity changes (Chen et al., 2014; Lee et al., 2013; Turrigiano, 2012). LTP/LTD and homeostatic plasticity are expressed through changes in AMPAR localization and function, and alterations in these mechanisms are implicated in nervous system disorders, including Alzheimer's disease, schizophrenia, Down syndrome, and autism.

AMPARs are tetrameric assemblies of the GluA1–Glut4 subunits forming glutamate-gated channels that are permeable to Na^+, K^+, and sometimes Ca^{2+} (Traynelis et al., 2010). Because of post-transcriptional mRNA editing, GluA2 subunits differ from other GluA

subunits by introduction of Arg instead of Gln in the ion-conducting pore. The presence of this large, positively charged Arg renders GluA2-containing AMPARs impermeable to Ca^{2+} (Ca^{2+}-impermeable AMPARs [CI-AMPARs]) and with decreased conductance. In contrast, GluA2-lacking AMPARs, such as GluA1 homomers, are Ca^{2+}-permeable (CP-AMPARs) and have greater conductance.

Although GluA1 CP-AMPARs are excluded basally from hippocampal CA1 synapses, except very early in development (Lu et al., 2009; Rozov et al., 2012; Stubblefield and Benke, 2010), LTP/LTD and homeostatic plasticity can modify synaptic strength via insertion of CP-AMPARs (Aoto et al., 2008; Lu et al., 2007; Park et al., 2016; Plant et al., 2006; Sanderson et al., 2016, 2018; Soares et al., 2013; Sutton et al., 2006; Thiagarajan et al., 2005; Yang et al., 2010; but see Adesnik and Nicoll, 2007; Ancona Esselmann et al., 2017; Gray et al., 2007)). When recruited to synapses, CP-AMPARs influence plasticity expression and confer changes in plasticity signaling mechanisms, resulting in metaplasticity. Importantly, CP-AMPAR-mediated metaplasticity at striatal and amygdalar synapses has been linked to drug addiction and fear extinction, respectively (Clem and Huganir, 2010; Wolf and Tseng, 2012). In addition, intracellular exposure to synaptotoxic β-amyloid (Aβ)(1–42) oligomers can recruit CP-AMPARs to hippocampal CA1 synapses (Whitcomb et al., 2015). However, the roles of CP-AMPARs in controlling hippocampal plasticity remain controversial, in large part because we do not have an adequate understanding of the mechanisms regulating CP-AMPARs.

Accumulating evidence indicates that the cyclic AMP (cAMP)-dependent protein kinase (PKA) and the Ca^{2+}-dependent protein phosphatase Calcineurin (CaN) play key roles regulating GluA1 and CP-AMPARs during synaptic plasticity, in part by controlling GluA1 phosphorylation (Diering et al., 2014; Goel et al., 2011; Kim and Ziff, 2014; Lu et al., 2007; Park et al., 2021; Sanderson et al., 2012, 2016; Soares et al., 2013; Yang et al., 2010). In addition, several studies have implicated CaN-LTD signaling in contributing to synaptic depression, LTP inhibition, and cognitive impairment following exposure to Aβ oligomers that accumulate in Alzheimer's disease (D'Amelio et al., 2011; Dineley et al., 2007, 2010; Hsieh et al., 2006; Jo et al., 2011; Kim et al., 2015; Reese et al., 2008; Shankar et al., 2007; Taglialatela et al., 2009, 2015; Wu et al., 2010; Yamin, 2009; Zhao et al., 2010). In the case of PKA signaling, the conclusions of previous studies are mixed, with some implicating PKA in Aβ-mediated synaptic dysfunction and others finding that PKA protects against deleterious effects of Aβ (Li et al., 2013; Vitolo et al., 2002; Wang et al., 2009, 2013; Whitcomb et al., 2015). However, previous studies of PKA and CaN in Aβ-mediated synaptic dysfunction primarily relied on pharmacological manipulation of cAMP levels or kinase and phosphatase activities that would globally affect all PKA or CaN signaling, including pre- and postsynaptic.

In contrast, studies from our laboratory and others found that highly localized postsynaptic anchoring of PKA and CaN to A-kinase anchoring protein (AKAP) 79/150 (79, human/150, rodent) is crucial for coordinating bi-directional control of CP-AMPAR incorporation at hippocampal synapses (reviewed in Purkey and Dell'Acqua, 2020). Our previous studies analyzed *in vitro* cultures and *ex vivo* brain slices from juvenile mice with knockin mutations in the *Akap5* gene that disrupted AKAP150 anchoring of PKA (150ΔPKA)

or CaN (150ΔPIX). In particular, PKA anchoring disruption prevented recruitment of CP-AMPARs to synapses, leading to impaired homeostatic potentiation *in vitro* and reduced LTD but normal LTP in area CA1 *ex vivo*. In contrast, CaN anchoring disruption increased basal synaptic incorporation of CP-AMPARs to prevent homeostatic potentiation *in vitro* but result in enhanced CA1 LTP and impaired LTD *ex vivo* (Sanderson et al., 2012, 2016, 2018). However, our prior work and studies by others indicate that the role of CP-AMPARs in plasticity is itself plastic and strongly influenced by inducing stimulus and postnatal development (reviewed in Purkey and Dell'Acqua, 2020). Thus, the roles of AKAP-anchored PKA and CaN in controlling CP-AMPARs and LTP/LTD balance could be different in adults, when synaptic development is complete, compared with juveniles, when synapses are still forming and maturing. Accordingly, here we characterized CP-AMPAR regulation during synaptic plasticity at CA1 synapses in adult wild-type (WT), 150ΔPKA, and 150ΔPIX mice under normal conditions and following exposure to Aβ(1–42) oligomers to reveal crucial roles of AKAP-PKA/CaN signaling in regulating LTP/LTD balance and how it is disrupted by Aβ.

RESULTS

Genetic disruption of AKAP-CaN anchoring leads to increased basal incorporation of CP-AMPARs at CA1 synapses in adult mice

We first sought to characterize basal glutamatergic excitatory synaptic input to CA1 neurons using whole-cell recording in *ex vivo* hippocampal slices prepared from 8- to 16-week-old adult 150ΔPKA and 150ΔPIX mice compared with WT controls (Figure 1). We observed no changes in the mean amplitude (Figures 1A and 1B) or frequency (Figures 1A and 1C) of spontaneous excitatory postsynaptic currents (sEPSCs) mediated by AMPARs compared with the WT in ΔPKA ($p = 0.69$ amplitude, $p = 0.98$ frequency) or ΔPIX mice ($p = 0.78$ amplitude, $p = 0.99$ frequency; one-way ANOVA with Dunnett's). We next assessed the ratio of AMPAR to NMDAR-mediated basal synaptic transmission in CA1 neurons in response to stimulation of the Schaffer collateral (SC) inputs from CA3 (Figures 1D–1F). The amplitude of the evoked AMPAR EPSC was measured as the peak of the response recorded at −65 mV (fast inward AMPA current) or +40 mV (fast outward AMPA plus some NMDA current). The amplitude of the evoked NMDAR EPSC was measured 70 ms after onset of the outward +40 mV response, when the faster AMPAR response had largely decayed (Figure 1D). Although the −65 mV and +40 mV AMPA/NMDA EPSC ratios were unchanged for 150ΔPKA mice (Figure 1E, $p = 0.74$; Figure 1F, $p = 0.85$), these ratios were increased significantly for 150ΔPIX compared with the WT (Figure 1E, ****$p < 0.0001$; Figure 1F, **$p = 0.006$; one-way ANOVA with Dunnett's).

An increased AMPA/NMDA EPSC ratio in ΔPIX mice could result from increased AMPAR transmission, decreased NMDAR transmission, a change in AMPAR subunit composition, and/or a combination of the above. Consistent with some amount of increase in AMPA/NMDA ratio for ΔPIX being due to decreased NMDAR-mediated transmission, the mean amplitude of the +40 mV NMDA EPSC measured 70 ms after onset was decreased (~56%) in ΔPIX CA1 neurons compared with the WT (Figure 1G; **$p = 0.006$ by one-way ANOVA with Dunnett's test). However, the increase in the inward −65 mV AMPA/NMDA ratio

was substantially larger (~130%; Figure 1E) than the increase in the outward +40 mV AMPA/NMDA ratio (~36%; Figure 1F) observed for 150ΔPIX. Thus, this differential effect on the inward versus outward AMPA/NMDA EPSC ratios in ΔPIX mice cannot solely be accounted for by decreased NMDAR transmission, which would affect these two ratios equally. Consistent with the measurements of sEPSC amplitude and frequency above, dendritic spine densities in the CA1 *stratum radiatum*, assessed by Golgi staining, were also not significantly different for ΔPIX compared with the WT (Figures 1H and 1I; $p = 0.22$ by one-way ANOVA with Dunnett's). Thus, the increases in evoked AMPA/NMDA ratio in 150ΔPIX also cannot be attributed to an increase in the number of excitatory synaptic connections on CA1 neurons. However, consistent with previous findings in juvenile mice (Lu et al., 2011; Sanderson et al., 2016), CA1 dendritic spine density was increased ~20% in adult 150ΔPKA compared with WT mice (Figures 1H and 1I; ***$p = 0.0005$ by one-way ANOVA with Dunnett's).

CP-AMPARs are sensitive to blockade of inward current by exogenous polyamine toxins and of outward current by endogenous polyamines, with the latter leading to a non-linear, inwardly rectifying current-voltage (I-V) response. In contrast, GluA2-containing CI-AMPARs display linear I-V responses and are insensitive to polyamines (Traynelis et al., 2010). Thus, our observations of a greater increase in inward −65 mV relative to outward +40 mV AMPA/NMDA EPSC ratios for ΔPIX suggest a possible increase in the basal contribution of inwardly rectifying GluA2-lacking CP-AMPARs, a finding that would be similar to that in juvenile ΔPIX mice (Sanderson et al., 2012, 2016). To further examine whether the subunit composition of synaptic AMPARs is altered basally in adult ΔPIX mice, we blocked NMDARs (10 μM (5S,10R)-(+)-5-methyl-10,11- dihydro-5H-dibenzo[α,δ]cyclohepten-5,10-imine maleate [MK801]) and recorded pharmacologically isolated, evoked SC-CA1 AMPAR EPSC responses across a range of holding potentials from −65 mV to +40 mV (Figure 2A). Importantly, inward rectification of synaptic AMPAR responses was evident for 150ΔPIX but not 150ΔPKA or the WT in normalized I-V plots of EPSC responses (Figure 2B; **$p = 0.007$, ***$p < 0.0001$ to WT by 2-way ANOVA with Bonferroni's) and in measurements of EPSC rectification indices calculated as the ratio of the inward to the outward AMPAR EPSC amplitudes at −65 mV and +40 mV, respectively (Figure 2C; ****$p < 0.0001$ to WT by one-way ANOVA with Dunnett's). To independently assess contributions of CP-AMPARs to basal transmission, we also recorded inward −65 mV AMPAR EPSC responses before and after application of the CP-AMPAR polyamine antagonist N,N,H,-trimethyl-5-[(tricyclo[3.3.1.13,7]dec-1-ylmethyl)amino]-1-pentanaminiumbromide hydrobromide (IEM1460; 70 μM) and found that IEM1460 (IEM) significantly decreased EPSC amplitude only for ΔPIX (~22%) and had no effect on responses in the WT or ΔPKA (Figure 2D; **$p = 0.009$ to WT by one-way ANOVA with Dunnett's). Thus, based on multiple criteria, genetic disruption of AKAP-CaN anchoring resulted in an aberrant increase in basal incorporation of CP-AMPARs at SC-CA1 synapses in adult ΔPIX mice. Also consistent with previous findings, our results indicate that CP-AMPARs do not make appreciable contributions to basal SC-CA1 synaptic transmission in WT mice (Lu et al., 2009; Rozov et al., 2012; Sanderson et al., 2016).

Genetic disruption of AKAP-PKA anchoring prevents CP-AMPAR synaptic incorporation to reduce LTP and shift expression primarily to CI-AMPARs

To determine the effects of genetic disruption of AKAP-PKA and CaN anchoring on synaptic plasticity in adult mice, we first turned to extracellular recording of field excitatory postsynaptic potentials (fEPSPs) for SC-CA1 synapses in the *stratum radiatum* of acute slices. Assessment of basal transmission by determining input-output (I-O) relationships for fEPSP slope versus presynaptic stimulus intensity showed no difference between the WT and ΔPIX but did reveal a significant increase in the I-O curve for ΔPKA compared with the WT (Figure S1A; $^{**}p < 0.01$ to $^{****}p < 0.0001$ by one-way ANOVA with Bonferroni's), which was somewhat unexpected based on the whole-cell recording data above showing normal sEPSC activity (Figures 1A–1C) and AMPA/NMDA EPSC ratios for ΔPKA (Figures 1D–1F). However, this increase in the fEPSP I-O curve for ΔPKA was not related to any change in the probability of presynaptic glutamate release, as shown by similar paired-pulse facilitation ratios for all three genotypes (Figure S1B), indicating that it is likely postsynaptic in nature and, at least in part, possibly related to the increase in CA1 *stratum radiatum* dendritic spine density/excitatory synapse number noted above (Figures 1H and 1I).

Despite these changes in basal transmission, adult ΔPKA and ΔPIX mice exhibited robust LTP of fEPSP responses induced by a single 1-s, 100-Hz high-frequency stimulus (HFS) train, with no difference compared with the WT in the level of expression ~30 min after induction for ΔPIX (Figure 3A) but a moderate decrease (~25% < WT) measured for ΔPKA (Figure 3B; $^{***}p < 0.001$ to WT by 2-way ANOVA). Significantly decreased LTP expression (~33% < WT) was also observed for 150ΔPKA at later time points (~90 min) after induction in independent experiments (Figure 3C; $^{***}p < 0.001$ by 2-way ANOVA). In agreement with previous work by others in adult mice (Lu et al., 2007), LTP induced by 1 × 100-Hz HFS in 8- to 16-week-old WT mice was heavily dependent on CP-AMPAR recruitment, as shown by a substantial reduction (~56%) in expression when IEM was added immediately after induction (Figure 3D; $^{***}p < 0.001$ by 2-way ANOVA). Similar inhibition (~58%) of LTP expression by IEM was also observed for 150ΔPIX (Figure 3E; $^{***}p < 0.001$ by 2-way ANOVA), indicating that CP-AMPARs also prominently support LTP in these mice. In contrast, LTP expression in 150ΔPKA was not sensitive to inhibition by IEM (Figure 3F; $p = 0.085$ by 2-way ANOVA), indicating that the reduced level of LTP expression observed in these mice is supported almost entirely by GluA2-containing CI-AMPARs. Furthermore, these results indicate that AKAP-anchored PKA signaling is required for effective recruitment of CP-AMPARs to CA1 synapses during LTP.

Although our fEPSP LTP recording results for adult WT and ΔPKA mice are fairly similar to previous findings in ~2-week-old juveniles, where we also observed CP-AMPAR-dependent expression of 1 × 100-Hz LTP in WT mice and a shift toward CI-AMPAR-dependent expression in ΔPKA mice, our current findings in adult ΔPKA mice are somewhat complicated by the increased fEPSP I-O relationship (Figure S1A). Therefore, we sought to independently characterize LTP using a whole-cell recording approach that also allowed us to directly monitor synaptic recruitment of CP-AMPARs. Importantly, our whole-cell recordings above revealed no differences in evoked AMPAR- and NMDAR-

mediated basal transmission at SC-CA1 synapses for adult ΔPKA mice (Figures 1 and 2). Accordingly, we monitored SC-CA1 AMPAR EPSC responses (isolated in the presence of picrotoxin to block $GABA_A$ receptors) recorded every 20 s at a holding potential of −65 mV during a 3-min baseline period (immediately after establishing whole-cell access) and then induced LTP by first depolarizing the postsynaptic CA1 neuron to 0 mV for 90 s with ongoing basal stimulation, followed by an additional 90 s of 3 Hz stimulation of the presynaptic SC inputs (Brachet et al., 2015), before returning to −65 mV to monitor post-induction EPSC responses (Figure 4A). In WT neurons, LTP expression developed over the next ~6 min after delivery of this induction stimulus and then was maintained stably for at least 20 min (Figure 4A). Although similar levels of LTP expression resulted from this induction protocol for 150ΔPIX compared with the WT (Figure 4A; $p = 0.42$), LTP expression was strongly reduced (~66% < WT) for 150ΔPKA (Figure 4A; ****$p < 0.0001$ to WT by 2-way ANOVA). Consistent with CP-AMPAR recruitment to CA1 synapses supporting LTP expression, application of the CP-AMPAR antagonist N-[3-[[4-[(3Aminopropyl)amino] butyl]amino]propyl]-1-naphthaleneacetamide trihydrochloride (NASPM; 20 μM) to WT slices fully prevented LTP expression induced by this pairing protocol, similar to application of a combination of NMDAR antagonists (MK801, 10 μM; D-2-amino-5-phosphonovaleric acid [D-APV], 50 μM), the latter confirming the NMDAR dependence of induction (Figure 4B; ****$p < 0.0001$ to WT control by 2-way ANOVA and one-way ANOVA with Bonferroni's).

In similar experiments, we also periodically recorded outward EPSC responses at a holding potential of +60 mV and then calculated an AMPAR EPSC rectification index as the ratio of the peaks of the inward −65 mV and outward +60 mV responses (Figure 4C). Although this ratio does not provide a pure measurement of AMPAR rectification because of some contamination of the peak of the fast, outward AMPAR EPSC by the rising phase of the slower, outward NMDAR EPSC and partial relief of the polyamine block of the outward current at +60 mV, it does provide a meaningful approximation of AMPAR rectification (Sanderson et al., 2016). Importantly, in WT neurons, this AMPAR rectification index increased significantly immediately following delivery of the pairing induction stimulus and remained elevated out to 10 min after induction, indicating that CP-AMPARs are being recruited to WT SC-CA1 synapses to support LTP expression (Figure 4C; *$p = 0.04$, **$p = 0.004$, **$p = 0.007$, ****$p < 0.0001$ to Before by one-way ANOVA with Dunnett's). In addition, CP-AMPAR and NMDAR antagonism prevented increased rectification after 3-Hz pairing stimulation (Figures 4D and 4E; $p = 0.67$ NASPM, $p = 0.76$ MK801/AP-V to Before by one-way ANOVA with Dunnett's). In further support of our conclusion that CP-AMPAR recruitment supports this form of LTP, the strongly impaired potentiation observed in ΔPKA mice was accompanied by failure to detect significantly increased AMPAR rectification at any time point following the induction stimulus (Figure 4F; $p = 0.11$ by one-way ANOVA). In contrast, the comparatively normal LTP observed in ΔPIX mice, like in WT mice, was inhibited completely by NASPM (Figure 4G; ****$p < 0.0001$ by 2-way ANOVA and one-way ANOVA with Bonferroni's) and was accompanied by persistent, unchanging elevation in AMPAR rectification (Figure 4H; $p = 0.13$ by one-way ANOVA). Importantly, in agreement with our more exact measurements of basal AMPAR rectification for ΔPIX above (Figures 2B and 2C), this approximate measurement of AMPAR rectification was

increased basally for ΔPIX compared with the WT even before LTP induction (Figure 4H; ####p < 0.0001 by one-way ANOVA with Dunnett's).

Genetic disruption of AKAP-PKA anchoring prevents transient CP-AMPAR recruitment that primes adult CA1 synapses for LTD mediated by AKAP-CaN signaling, which removes synaptic AMPARs

Our prior work found LTD impairments in ~2 week-old juvenile ΔPKA and ΔPIX mice that were, respectively, related to failed CP-AMPAR synaptic recruitment and subsequent failed removal during LTD induction in response to prolonged (6–15 min) 1-Hz low-frequency stimulation (LFS) (Sanderson et al., 2012, 2016). However, NMDAR-dependent LTD declines in magnitude over the course of postnatal development and becomes very difficult to induce *ex vivo* in hippocampal slices prepared from adult animals using standard 1-Hz LFS protocols. To overcome this difficulty we employed a modified, whole-cell recording protocol with GABAergic inhibition intact to favor LTD induction in adult mice (Steele and Mauk, 1999). We first monitored inward AMPAR EPSC responses at a holding potential of −40 to 30 mV (adjusted for each cell to be at/near the Cl^- reversal potential where little or no inward or outward $GABA_A$receptor current was detected) and next employed the same 0-mV, 3-Hz pairing stimulation used above to induce LTP but without including a $GABA_A$ receptor blocker (Brachet et al., 2015; Figure 4). We then returned to −40 to 30 mV to monitor AMPAR EPSC responses after induction and found that this modified 3-Hz stimulation protocol reliably induced long-lasting ~20% depression of AMPAR EPSC responses in adult WT slices that required NMDAR (Figure 5A; MK801/APV ****p < 0.0001 by 2-way ANOVA and one-way ANOVA with Bonferroni's) and CP-AMPAR activity (Figure 5B; NASPM ****p < 0.0001 by 2-way ANOVA and one-way ANOVA with Bonferroni's), both of which are similar to our previousfindings in juvenile mice (Sanderson et al., 2016). However, this stimulation protocol failed to induce any LTD in ΔPKA mice, consistent with impaired CP-AMPAR recruitment, and inappropriately resulted in synaptic potentiation/LTP in ΔPIX mice (Figure 5C; ****p < 0.0001 to WT by 2-way ANOVA and one-way ANOVA with Bonferroni's). Importantly, the aberrant potentiation we observed in adult ΔPIX mice was prevented by NASPM, consistent with failure to remove the additional CP-AMPARs recruited during LTD induction (Figure 5D; ****p < 0.0001 by 2-way ANOVA and one-way ANOVA with Bonferroni's). These findings indicate that, like in juveniles, AKAP-anchored PKA and CaN also control NMDAR-dependent LTD in adult animals through their dynamic, opposing control of CP-AMPAR synaptic incorporation and removal, respectively.

Inhibition of LTP by synaptotoxic Aβ oligomers requires AKAP-PKA and AKAP-CaN signaling

A major motivation for characterizing synaptic plasticity in adult ΔPKA and ΔPIX mice was so that we could lay the groundwork for investigating mechanisms underlying synaptic dysfunction in disorders that affect the adult brain, such as Alzheimer's disease. Accordingly, we next evaluated the effects of acutely exposing slices from adult WT, ΔPKA, and ΔPIX mice to synaptotoxic Aβ(1–42) oligomers prior to inducing LTP (Figure 6). Delivery of 2 × 100-Hz HFS, 1-s trains spaced 5 min apart induced an ~50% LTP of fEPSP slope in WT mice that was stably expressed for at least 60 min after induction

under control conditions (Figures 6A and 6F). Consistent with our prior work (Freund et al., 2016), this spaced 2 × HFS-induced LTP was almost completely absent in WT mouse slices exposed to 100 nM Aβ (Figures 6A, ****p < 0.0001 by 2-way ANOVA, and 6F, ***p = 0.0002 by one-way ANOVA with Bonferroni's). Similar to LTP induced with a single HFS (Figure 3F), expression of LTP induced by spaced 2 × HFS also required CP-AMPAR activity, as shown by nearly complete inhibition of stable expression by NASPM applied prior to and during induction and initial expression (Figures 6B, ****p < 0.0001 by 2-way ANOVA, and 6F, ****p < 0.0001 by one-way ANOVA with Bonferroni's). Delayed application of IEM after the spaced 2 × HFS induction stimulus also significantly reduced the subsequent level of LTP expression to ~30% (Figure 6F, **p = 0.0037 by one-way ANOVA with Bonferroni's), although this inhibition of LTP was not as complete as seen for NASPM applied during induction/initial expression, indicating that some replacement of recently recruited CP-AMPARs with CI-AMPARs likelyhas occurredbythistimeafter induction. Importantly, under control conditions in slices from 150ΔPKA mice, spaced 2 × HFS also induced stable LTP expression (~46%) that was similar in magnitude to that of the WT (Figure 6D, p = 0.56 by2-way ANOVA)but completelyinsensitive to inhibition by Aβ (Figures 6C, p = 0.87 by 2-way ANOVA, and 6F, p = 0.72 by one-way ANOVA with Bonferroni's) and by addition of IEM after induction, which instead increased LTP expression (~74%) compared with controls (Figure 6F, *p = 0.011 by one-way ANOVA with Bonferroni's). Although stable LTP induced by spaced 2 × HFS was somewhat elevated in magnitude in slices from ΔPIX (~77%) compared with the WT (~53%) under control conditions (Figure 6D; *p = 0.02 to WT by 2-way ANOVA), it was only partially inhibited by Aβ (Figures 6E, *p = 0.016 by 2-way ANOVA, and 6F, *p = 0.045 by one-way ANOVA with Bonferroni's) with robust expression still maintained at levels (~55%) similar to those observed for WT controls (~53%). However, LTP expression for ΔPIX was strongly reduced (to ~35%) by post-induction application of IEM (Figure 6F, ****p < 0.0001 by one-way ANOVA with Bonferroni's), indicating that this LTP expression depends on CP-AMPARs similar to in WT mice. Thus, surprisingly, LTP resists Aβ inhibition in adult ΔPKA and ΔPIX mice despite these mutations resulting in opposite effects on CP-AMPAR regulation during LTP.

Extracellular application of Aβ oligomers rapidly recruits CP-AMPARs to CA1 synapses via AKAP-PKA signaling to prime LTP inhibition mediated by AKAP-CaN signaling similarly as in LTD

Previous studies suggest that Aβ impairs LTP by favoring inappropriate activation of LTD signaling that opposes LTP (Hsieh et al., 2006; Jo et al., 2011; Reese et al., 2008; Shankar et al., 2007, 2008; Wu et al., 2010; Yamin, 2009; Zhao et al., 2010). To this end, the common resistance of ΔPKA and ΔPIX mice to Aβ inhibition of LTP could be related to the shared phenotype of impaired LTD observed above (Figure 5), where AKAP-PKA signaling normally promotes CP-AMPAR recruitment, which primes CA1 synapses to undergo LTD via subsequent AMPAR removal mediated by AKAP-CaN signaling downstream of CP-AMPAR Ca^{2+} influx (Sanderson et al., 2012, 2016; Figure 5). For this parallel between LTD and Aβ inhibition of LTP to apply here, the insensitivity of ΔPKA mice to Aβ inhibition of LTP could be related to failure of Aβ exposure to recruit CP-AMPARs to CA1 synapses to prime LTD signaling by AKAP-CaN. In support of this idea, a prior study found that

exposure to intracellular Aβ oligomers introduced through a patch pipette led to rapid PKA-mediated synaptic insertion of GluA1 CP-AMPARs in CA1 neurons (Whitcomb et al., 2015). To determine whether the extracellular Aβ treatment we and others typically employed to inhibit LTP also rapidly promotes CP-AMPAR synaptic incorporation, we used whole-cell recording to monitor changes in AMPAR rectification (in the presence of AP-V and MK801 to block NMDARs) after extracellular application of 100 nM Aβ oligomers. Consistent with rapid CP-AMPAR synaptic insertion, in slices from WT mice, extracellular Aβ triggered a significant increase (~50%) in the −65/+60 AMPA EPSC rectification index within min of application that was maintained over 30 min of recording (Figures 7A and 7B; **p = 0.003, **p = 0.007, ****p < 0.0001 by one-way ANOVA with Dunnett's). Interestingly, AMPAR rectification also increased substantially (~100%) in WT slices that were exposed simultaneously to Aβ and stimulated with a 3-Hz, 0-mV pairing LTP induction protocol under conditions where NMDARs were not blocked (Figures 7C and 7D; Before n = 7, 0 min n = 7, 3 min n = 7, 5 min n = 4; ***p < 0.001 to Before by one-way ANOVA with Dunnett's). However, instead of this pairing protocol and the resulting CP-AMPAR recruitment leading to LTP, as shown above for WT mice under control conditions (Figures 4A and 4B), it resulted in LTD of ~20% in the presence of Aβ (Figure 7E; ****p < 0.0001 0–3 min, n = 8 compared with 27–30 min, n = 8 by 2-way ANOVA). These striking results are consistent with the idea proposed above that CP-AMPARs promote LTD at the expense of LTP in the presence of Aβ in WT mice.

In contrast to WT mice (Figures 7A and 7B), extracellular Aβ failed to increase AMPAR rectification in ΔPKA mice even after 30 min of exposure (Figures 7F and 7G; p = 0.76 by one-way ANOVA). Consistent with the independent measurements above (Figures 3 and 4G), the −65/+60 AMPA EPSC rectification index in ΔPIX slices was already increased basally compared with the WT before Aβ application (Figures 6H and 6I; ####p < 0.0001 to WT Before by one-way ANOVA with Dunnett's) and did not increase further after Aβ application (Figures 6H and 6I; p = 0.086 by one-way ANOVA) but was maintained at elevated levels similar to those observed for WT slices after Aβ application. Interestingly, in these same experiments, the increased AMPAR rectification induced by Aβ in the WT was not accompanied by potentiation of the inward −65 mV AMPA EPSC, indicating that the CP-AMPARs recruited by Aβ are replacing CI-AMPARs to result in no net change in synaptic strength (Figures 6A and 6J). However, in contrast to the lack of change in basal synaptic strength seen in the WT and also ΔPKA (Figures 6F and 6J), slices from ΔPIX mice exhibited rapid AMPA EPSC potentiation following Aβ application (Figures 6H and 6J; ****p < 0.0001 by 2-way ANOVA to WT) despite the lack of any further increase in rectification (Figures 6H and 6I). Thus, in ΔPIX mice, Aβ appears to cause LTP-like incorporation of CP-AMPARs and CI-AMPARs to increase synaptic strength.

Importantly, these results also support the model proposed above where, similar to during LTD induction, Aβ exposure promotes CP-AMPAR incorporation via AKAP-PKA signaling, which primes synapses for enhanced AKAP-CaN signaling to favor subsequent CP-AMPAR and CI-AMPAR removal to prevent LTP expression. According to this model, resistance to Aβ inhibition of LTP in ΔPIX mice would be due to impaired CP-AMPAR activation of CaN signaling, which removes AMPARs from synapses, whereas resistance to Aβ inhibition of LTP in ΔPKA mice would be due to failure of PKA signaling, which

recruits CP-AMPARs to prime synapses for overactivation of AKAP-CaN/LTD signaling. Based on the insensitivity to Aβ inhibition of LTP in ΔPKA mice, which cannot recruit CP-AMPARs, a prediction of this model is that LTP induced in WT mice under conditions that do not require CP-AMPAR recruitment for expression should also be insensitive to Aβ inhibition. Importantly, our results above (Figures 3 and 6) and prior studies indicate that CA1 LTP in adult rodents induced with a single HFS or theta burst (TBS) train or multiple HFS/TBS trains spaced apart by several minutes is sensitive to CP-AMPAR and PKA inhibition, whereas LTP induced by multiple, massed HFS/TBS trains that are only separated by seconds is insensitive to CP-AMPAR and PKA inhibition (Gray et al., 2007; Lu et al., 2007; Park et al., 2016, 2021). Accordingly, in adult WT mice, we found that LTP induced by 2 × 100-Hz, 1-s trains spaced only 10 s apart was insensitive to inhibition by Aβ and NASPM, whether added separately or together (Figures 7H, $p = 0.77$ Aβ, $p = 0.23$ Aβ+NASPM by 2-way ANOVA, and 7I, $p = 0.99$ Aβ, $p = 0.93$ Aβ+NASPM, ***$p = 0.0001$ NASPM [increased] to control by one-way ANOVA with Dunnett's). Thus, the mechanisms by which Aβ impairs LTP are heavily intertwined with the postsynaptic AKAP-anchored PKA/CaN signaling pathways that control normal LTP/LTD balance through opposing regulation of CP-AMPAR synaptic recruitment and removal.

DISCUSSION

GluA1 CP-AMPAR regulation of synaptic plasticity changes over the course of postnatal development

The role of GluA1 and CP-AMPARs in regulating synaptic plasticity at CA1 synapses remains controversial, with a number of conflicting studies in the literature, some reporting GluA1 and CP-AMPAR dependence of LTP (Esteban et al., 2003; Guire et al., 2008; Lee et al., 2003; Lu et al., 2007; Park et al., 2016, 2021; Plant et al., 2006; Purkey et al., 2018; Sanderson et al., 2016; Yang et al., 2010; Zhou et al., 2018) and others not (Adesnik and Nicoll, 2007; Granger et al., 2013; Gray et al., 2007; reviewed in Buonarati et al., 2019; Purkey and Dell'Acqua, 2020). However, most prior studies of CP-AMPAR regulation of LTP/LTD examined juvenile animals, where CA1 synapses are undergoing developmental changes. Importantly, the dependencies of LTP on GluA1 subunits, probed using genetic approaches, and on CP-AMPAR activity, probed using pharmacologic approaches, change over the course of postnatal development and also exhibit robust compensation in the face of genetic manipulation (Jensen et al., 2003; Kolleker et al., 2003; Lee et al., 2003; Lu et al., 2007; Sanderson et al., 2016; Zamanillo et al., 1999). Indeed, prior studies found that, although PKA-dependent synaptic recruitment of CP-AMPARs can contribute prominently to 1 × 100-Hz LTP in WT mice younger than 2 weeks, this CP-AMPAR dependence disappears over the next 4–7 days of development before reappearing in adult animals older than 8 weeks (Figure 3; Lu et al., 2007; Sanderson et al., 2016). Likewise, it is very clear that genetic knockout of GluA1 and deleting or mutating its C-terminal phosphorylation sites can have comparatively little effect on LTP in mice ~2–3 weeks of age but result in substantial LTP impairment in adults (Granger et al., 2013; Jensen et al., 2003; Kolleker et al., 2003; Lee et al., 2003; Zamanillo et al., 1999). Furthermore, recruitment of CP-AMPARs to CA1 synapses even at a single developmental age depends on the inducing stimulus employed (Figure 7; Guire et al., 2008; Lu et al., 2007; Park et al., 2016, 2021;

Purkey et al., 2018). Thus, much of the controversy regarding regulation of CA1 plasticity by GluA1 CP-AMPARs is likely rooted in differences in one or more of these variables across studies (reviewed in Purkey and Dell'Acqua, 2020).

Of particular relevance here, prior work found that, although AKAP150-PKA anchoring and GluA1 S845 phosphorylation are required for LTD expression in juvenile animals and can contribute to LTP in adult animals (Figures 3 and 4), they are dispensable for LTP expression in juveniles (He et al., 2009; Lee et al., 2003, 2010; Lu et al., 2007). These observations are consistent with other findings indicating that LTP in its most fundamental form involves structural rearrangements of the postsynaptic density (PSD) to create additional slots that can be filled by AMPARs, independent of subunit composition, that exchange with a reserve pool of extrasynaptic receptors cycling through endosomes (Choquet, 2018; Granger et al., 2013; Herring and Nicoll, 2016; Kennedy et al., 2010; Nair et al., 2013; Opazo et al., 2010, 2012; Park et al., 2004; Penn et al., 2017; Petrini et al., 2009; Sinnen et al., 2017; Tang et al., 2016). However, it appears that the subunit composition of AMPARs already present in and/or delivered to this reserve pool changes during development, is regulated by AKAP-PKA/CaN signaling balance, and depends on the induction stimulus employed.

AKAP-PKA/CaN regulation of CP-AMPARs plays a crucial role in metaplastic regulation of LTP/LTD balance in the juvenile and adult hippocampus despite developmental changes

Given all of the abovementioned developmental plasticity, we thought that, to understand diseases that affect the adult brain, such as Alzheimer's disease, we needed to examine how genetic disruption of AKAP150-anchored PKA and CaN signaling affects CP-AMPAR regulation in the mature hippocampus when synaptic development is complete. Accordingly, here we found that AKAP150 scaffolding of the opposing PKA and CaN signaling pathways regulates LTP and LTD by controlling the balance of CP-AMPAR insertion and removal at adult CA1 synapses and that this bi-directional regulation is also central to the mechanism by which Aβ inhibits LTP. Although CA1 LTP is induced easily by various patterns of 100-Hz HFS in extracellular fEPSP recordings in slices prepared from juvenile and adult rodents, CA1 LTD has traditionally been difficult to induce *ex vivo* in adults. In addition, CA1 LTP is not commonly studied using whole-cell recording in adults. Importantly, in addition to characterizing CP-AMPAR regulation in LTP induced by various HFS protocols in fEPSP recordings, here we also employed a modified whole-cell recording approach using 3-Hz stimulation with $GABA_A$ receptor-mediated inhibition blocked to favor LTP induction and then intact to facilitate LTD induction. Using these approaches, we found that the roles of AKAP-PKA and CaN anchoring in regulating CP-AMPARs in LTD are roughly similar in adults and juveniles, with CP-AMPAR antagonists blocking LTD in WT mice and 150ΔPKA and 150ΔPIX mice failing to express LTD (Sanderson et al., 2012, 2016). In addition, we found that genetic disruption of CaN anchoring in adult ΔPIX mice, like in juveniles, basally increased CP-AMPARs at CA1 synapses, and LTD induction not only failed to remove these CP-AMPARs but also resulted in further CP-AMPAR recruitment, leading to inappropriate potentiation.

Somewhat in contrast to juvenile ΔPKA mice, where LTP expression levels were unaffected, we found that genetic disruption of PKA anchoring in adults resulted in reduced 1 × 100-Hz and 3-Hz pairing LTP expression, along with a corresponding failure to recruit CP-AMPARs to the synapse. In addition, we found that the 1 × 100-Hz LTP expression remaining in ΔPKA mice, unlike in the WT, was insensitive to CP-AMPAR antagonism. Although use of a stronger, spaced 2 × 100-Hz HFS induction protocol could largely rescue the LTP expression deficits in ΔPKA compared with WT adults, this spaced 2 × HFS LTP prominently required CP-AMPAR activity in WT but not ΔPKA mice. Thus, LTP expression in 150ΔPKA adults, like in juveniles, has shifted to be mediated primarily by CI-AMPARs. Finally, we found that disruption of CaN anchoring did not result in enhanced 1 × 100-Hz LTP in adults like it did in juveniles; however, we did observe slightly enhanced LTP in ΔPIX mice when induced with spaced 2 × HFS. This finding, combined with our observation that the pairing stimulus used to induce LTD in WT mice inappropriately resulted in CP-AMPAR-mediated potentiation in ΔPIX mice, is consistent with the idea that AKAP-anchored CaN also constrains LTP in adults by restricting CP-AMPAR synaptic incorporation.

Aβ inhibits LTP via AKAP-PKA signaling, which recruits CP-AMPARs to create a metaplastic state primed for AKAP-CaN signaling-mediated LTD

Overall, adult 150ΔPKA and 150ΔPIX mice exhibited metaplastic shifts in net LTP/LTD balance toward LTP and away from LTD. Importantly, this common directional shift in LTP/LTD balance, despite being caused by opposing effects on synaptic CP-AMPAR recruitment/removal, was able to confer resistance to Aβ-mediated inhibition of LTP in both mouse lines. Furthermore, our results indicate that this convergence in resistance to Aβ requires mechanisms very similar to LTD, where AKAP-PKA-mediated CP-AMPAR recruitment primes synapses for subsequent AKAP-CaN-mediated AMPAR removal to favor synaptic depression over potentiation (Sanderson et al., 2016). In particular, during LTD induction, AKAP-PKA signaling is engaged downstream of NMDARs, potentially through cAMP generated by Ca^{2+}-activated adenylyl cyclase scaffolded to AKAP79/150 (Efendiev et al., 2010; Willoughby et al., 2010), to selectively recruit CP-AMPARs, but not CI-AMPARs, to the synapse. This preferential effect of AKAP-PKA signaling on CP-AMPARs may be related to the presence of four S845 phosphorylation sites in a GluA1 homomer compared with only two in a GluA1/2 heteromer and could also be facilitated by the absence of any additional regulatory mechanisms imposed by GluA2 in a GluA1 homomer. However, at the same time, the low level of Ca^{2+} influx during LTD induction from NMDARs as well as the newly recruited CP-AMPARs also activates AKAP-CaN signaling to rapidly remove the newly recruited CP-AMPARs as well as CI-AMPARs, preventing potentiation and promoting LTD (Sanderson et al., 2016). In addition, CaN activation of DAPK1 during LTD induction is known to prevent Ca^{2+}/calmodulin-dependent protein kinase II (CaMKII) translocation to synaptic NMDARs, which is required for prolonged AMPAR recruitment, which, in turn, is required for LTP maintenance (Barcomb et al., 2016; Goodell et al., 2017; Halt et al., 2012; Sanhueza et al., 2011). Thus, during LTD induction, synapses never reach a state of synaptic potentiation despite CP-AMPAR recruitment because CaN signaling is constantly removing the newly recruited CP-AMPAR receptors and also preventing CaMKII from signaling bound to NMDARs as it does during LTP. However, when AKAP-CaN

anchoring is disrupted in ΔPIX mice, LTD induction can inappropriately result in LTP, at least in part because of failure to remove CP-AMPARs from the synapse (Figure 4). Based on our past (Sanderson et al., 2016) and present findings, ΔPKA mice fail to express LTD because of an inability to recruit CP-AMPARs to CA1 synapses, which are needed to boost Ca^{2+} activation of CaN signaling required for effective removal of pre-existing CI-AMPARs. In contrast to LTD, which only transiently recruits CP-AMPARs to CA1 synapses during induction, it is well established that LTP induction can more persistently recruit CPand CI-AMPARs to support its stable expression. During LTP induction, higher levels of NMDAR Ca^{2+} influx strongly activate AKAP-PKA and CaMKII signaling, which promote AMPAR recruitment, but only briefly engage opposing AKAP-CaN signaling, allowing translocation of CaMKII to NMDARs and robust synaptic incorporation of CP- and CI-AMPARs, with CP-AMPARs eventually being replaced by additional CI-AMPARs to maintain expression (Plant et al., 2006; Yang et al., 2010).

Although previous studies of acute synaptic dysfunction caused by Aβ oligomers have broadly implicated PKA, CaN, GluA1, and CP-AMPARs in the underlying signaling alterations (Hsieh et al., 2006; Shankar et al., 2007; Whitcomb et al., 2015; Zhao et al., 2010), we can now more clearly link these players in a specific CP-AMPAR regulatory pathway that closely mirrors the one that occurs during LTD. Furthermore, our findings provide additional support for models proposing that Aβ drives synaptic dysfunction through inappropriate engagement of LTD signaling (Hsieh et al., 2006; Jo et al., 2011; Li et al., 2011; Reese et al., 2008; Shankar et al., 2007, 2008; Sinnen et al., 2016; Wu et al., 2010; Yamin, 2009; Zhao et al., 2010). Our findings also allow us to conclude that postsynaptic cAMP-PKA signaling works in concert with Ca^{2+}-CaN signaling to help mediate, instead of protect against, the acute synaptotoxic effects of Aβ despite PKA and CaN opposing each other in regulation of CP-AMPAR synaptic trafficking. In particular, AKAP-PKA signaling recruits CP-AMPAR to create a metaplastic state induced by Aβ that is primed for LTD to prevail over LTP signaling, as shown most dramatically in Figure 7 for WT mice, where Aβ exposure was able to convert an LTP-inducing stimulus into an LTD-inducing stimulus despite similar increases in CP-AMPAR-mediated EPSC rectification.

Interestingly, we previously observed a similar metaplastic state favoring LTD over LTP in juvenile AKAP150CS knockin mice, where palmitoylation of the N-terminal membrane targeting domain was disrupted, resulting in loss of AKAP trafficking through recycling endosomes and a decrease in its association with the PSD (Purkey et al., 2018). In these AKAP150CS mice, we also observed a basal increase in CP-AMPAR incorporation that prevented LTP when induced with protocols that relied on CP-AMPAR recruitment for expression but allowed LTP when induced with a protocol that instead recruited CI-AMPARs for expression. These previous findings in AKAP150CS mice indicate that AKAP-PKA/CaN signaling in recycling endosomes and the PSD are likely crucial for supporting additional CP-AMPAR synaptic recruitment during LTP but that AKAP-PKA/CaN signaling in the extrasynaptic membrane is likely sufficient for CP-AMPAR removal from synapses during LTD. Importantly, here we found that induction of LTP with spaced 2 × HFS that relied on CP-AMPARs for expression in adult WT mice was sensitive to Aβ inhibition, whereas induction of LTP with a massed 2 × HFS protocol that only relied on CI-AMPARs for expression was insensitive to Aβ. Thus, paradoxically, although CP-

AMPAR recruitment can contribute positively to LTP expression, it also renders synapses vulnerable to Aβ-mediated synaptic dysfunction, which hijacks CP-AMPAR LTD regulatory mechanisms to inhibit LTP.

Overall, our findings demonstrate the importance of postsynaptic AKAP-PKA/CaN signaling balance in regulating not only LTP and LTD under normal conditions but also Aβ-mediated impairment of LTP. Importantly, this knowledge sets the stage for future exploration of aberrant AKAP-PKA/CaN regulation of CP-AMPARs in mediating Aβ disruption of hippocampal plasticity *ex vivo* and synapse loss and cognitive impairments associated with Alzheimer's disease *in vivo*. Of particular interest will be to determine the upstream mechanisms through which Aβ engages cAMP-AKAP-PKA and Ca^{2+}-AKAP-CaN signaling to control CP-AMPARs—are β_2-adrenergic receptors (Wang et al., 2013), mGlu5 receptors (Chen et al., 2017; Haas et al., 2014; Haas and Strittmatter, 2016; Wang et al., 2004), and/or endoplasmic reticulum (ER) Ca^{2+} and ryanodine receptors involved (Chakroborty et al., 2012a, 2012b; Goussakov et al., 2010; Popugaeva et al., 2017)? In addition, it will be important to determine where these Aβ-regulated signaling pathways converge on CP-AMPARs in terms of the different subcellular compartments through which AKAP79/150 and GluA1 are known to traffic dynamically; i.e., the PSD, extrasynaptic plasma membrane, and recycling endosomes (Keith et al., 2012; Purkey et al., 2018; Woolfrey et al., 2015).

STAR★METHODS

RESOURCE AVAILABILITY

Lead contact—Further information and requests for resources and reagents should be directed to and will be fulfilled by the Lead Contact, Mark Dell'Acqua, mark.dellacqua@cuanschutz.edu

Materials availability—We are glad to share the mouse lines used in this study with reasonable compensation by requestor for its processing and shipping. In addition, we may require a payment and/or a completed Materials Transfer Agreement if there is potential for commercial application.

Data and code availability—No standardized datatypes are reported in this paper. All other data reported in this paper will be shared by the lead contact upon request.

This paper does not report original code.

Any additional information required to reanalyze the data reported in this paper is available from the lead contact upon request.

EXPERIMENTAL MODEL AND SUBJECT DETAILS

All animal procedures were approved by the University of Colorado Anschutz Medical Campus Institutional Animal Care and Use Committee in accordance with National Institutes of Health (NIH)/United States Public Health Service guidelines. Production and initial characterization of AKAP150 ΔPIX mice and ΔPKA mice was previously described

in (Murphy et al., 2014; Sanderson et al., 2012, 2016), respectively. Both mouse alleles (AKAP150ΔPKA, RRID: MGI_5702316; AKAP150ΔPIX, RRID: MGI_5702308) were backcrossed to C57Bl6J several generations but then maintained, along with related WT controls, on a mixed C57Bl6J (75%)/ 129X1/SvJ (25%) background. Only male mice were used between 8–16 weeks of age due to well-characterized impacts of the estrous cycle leading to day-to-day variability in LTP. In addition, this study was initiated prior to NIH directives to consider sex as a biological variable.

METHOD DETAILS

Extracellular fEPSP recordings—Unless indicated, all chemicals were from Sigma-Aldrich. For slice preparation, 8–16 week-old mice were decapitated under deep anesthesia with isoflurane via inhalation. Alternatively, animals were cardiac-perfused with 50 mL of ice-cold cutting solution (in mM: 3 KCl, 1.25 $NaH2PO_4$, 12 $MgSO_4$, 26 $NaHCO_3$, 0.2 $CaCl_2$, 220 sucrose, 10 glucose) under deep anesthesia with ketamine. (250 mg/kg) prior to decapitation and then removal of the brain into 4°C cutting solution. The hippocampi were removed from the brain, and 400-μm-thick horizontal slices were made using a McIIwain tissue chopper. Slices were recovered at 22–27°C for > 80 min in ACSF/cutting solution mixture (ACSF in mm: 126 NaCl, 5 KCl, 2 $CaCl_2$, 1.25 NaH_2PO_4, 1 $MgSO_4$, 26 $NaHCO_3$, 10 glucose, and 2 N-acetyl cysteine). Following recovery, slices were transferred to a recording chamber and maintained at 29–30°C in ACSF minus N-acetyl cysteine. A bipolar tungsten stimulating electrode was placed in the SC pathway 200–300 μm from CA1 cell bodies to evoke fEPSPs recorded in the stratum radiatum using a nearby glass micropipette filled with ACSF (access resistance, 2–5 MΩ). Input-output (I-O) curves were measured by evoking fEPSPs at different intensities until the maximal response was determined by plotting initial fEPSP slope against stimulus intensity. For studies of LTP, the test stimulus intensity was set to evoke 40%–60% of the maximum slope and delivered at 0.05 Hz. The CP-AMPAR antagonists N,N,H,-trimethyl-5-[(tricyclo[3.3.1.13,7]dec-1-ylmethyl) amino]-1-pentanaminiumbromide hydrobromide (IEM1460) and N-[3-[[4-[(3Aminopropyl)amino] butyl]amino]propyl]-1-naphthaleneacetamide trihydrochloride (NASPM) and NMDAR antagonist (5S,10R)-(+)-5-Methyl-10,11- dihydro-5H-dibenzo[α,δ]cyclohepten-5,10-imine maleate (MK801) were purchased from Tocris. Aβ(1–42) was purchased from Anaspec and small, soluble oligomers were prepared as previously described (Freund et al., 2016). For experiments with Aβ, slices were recovered for 60 min and then preincubated with Aβ (100 nM) for > 60 min prior to LTP induction. Scope54 or WinLTP software was used for data acquisition and analysis.

Whole-cell electrophysiology—For whole-cell, voltage-clamp electrophysiological recordings, 300 μm horizontal hippocampal slices were prepared as above using a Vibratome. After 15 min recovery at 34°C, slices were then maintained at room temperature until recording. Whole-cell recordings were performed in a chamber maintained at 29–30°C and visualized using infrared–differential interference contrast microscopy. Patch-clamp electrodes had a resistance between 3 and 6 MΩ. Voltage-clamp recordings were obtained using an Axopatch 200B amplifier using pClamp software (Molecular Devices) at a holding potential of −65 mV, except as noted below for AMPA/NMDA evoked EPSC ratios, AMPAR rectification measurements, and LTD recordings. AMPAR sEPSCs isolated using

50 μm picrotoxin (Tocris) were recorded from CA1 pyramidal neurons using an intracellular solution (IS1) containing the following (in mM): 130 Cs gluconate, 1 CsCl, 1 $MgS0_4$, 10 HEPES, 1 EGTA, 4 MgATP, 0.4 MgGTP, and 2 QX-314, pH 7.3. Evoked EPSCs were recorded in whole-cell configuration; half-maximal stimulation was determined and then currents were evoked at holding potentials of −65 mV (inward AMPAR current) or +40 mV (outward AMPAR plus NMDAR current). Averaging recorded events (> 10/neuron) and overlaying the traces at −65 mV and +40 was used to determine AMPA/NMDA EPSC ratios as follows: AMPAR currents at +40 or −65 mV were measured from the peak amplitude of the EPSC and divided by NMDAR currents at +40 mV measured 70 ms after the onset of the EPSC. Normalized AMPAR EPSC I-V curves were obtained from averaged recordings (> 10/neuron) in the presence of 10 μM MK-801 and 50 μM picrotoxin extracellularly and spermine (10 μM) intracellular. Normalized I-V plots were generated from measurements of AMPAR EPSC peak amplitudes at different membrane holding potentials by dividing the mean AMPAR EPSC peak amplitude determined at −65 mV for each genotype. AMPAR rectification indices (RI) were obtained by dividing the peak amplitudes of AMPAR EPSCs recorded at −65 mV by those recorded at +40 mV or +60 mV for each neuron as indicated.

Whole-cell, voltage-clamp LTP experiments were recorded from CA1 pyramidal neurons using IS1 containing 10 μM spermine with 50 μM picrotoxin present in the AS*CF*. A bipolar tungsten-stimulating electrode was placed in the SC pathway 200 μM from the CA1 pyramidal cell to evoke EPSCs. After establishing whole-cell access, a 3-min gap-free baseline recording at −65 mV was performed and an EPSC rectification index (RI) of −65 mV (peak amplitude of inward AMPAR current)/+60 mV (peak amplitude of outward AMPAR plus contaminating NMDAR current) current was then determined. LTP was induced using a modified pairing protocol; cells were depolarized to 0 mV and held there for 90 s, with a pulse every 20 s, then LTP was induced by additional stimulation at 3 Hz for 90 s (Brachet et al., 2015). The cell was returned to −65 mV and evoked EPSC amplitudes were subsequently monitored every 20 s. RI values were also determined for 0, 3, 5, and 10 min post-LTP time-points. Similar recording approaches were used to assess the impact of Aβ(1–42) oligomers (100 nM) on AMPAR RI over time following 3 Hz LTP induction or in the presence of 10 μM MK-801 and 50 μM picrotoxin to fully isolate AMPA EPSC responses following application of Aβ(1–42) alone.

Whole-cell, voltage-clamp LTD experiments were recorded from CA1 pyramidal neurons using IS1 containing 10 μM spermine in the absence of picrotoxin extracellularly. A bipolar tungsten-stimulating electrode was placed in the SC pathway 200 μm from CA1 pyramidal cell to evoke EPSCs. After establishing whole-cell access, the reversal potential for GABAergic currents was determined for each cell (between −40 and −30 mV) and then membrane voltage was clamped at this potential to obtain a 3 min gap-free baseline recording. LTD was subsequently induced using the same 3 Hz stimulation protocol as described above to induce LTP (Brachet et al., 2015), but with GABAergic inhibition left unblocked to favor LTD induction (Steele and Mauk, 1999). The cell was then returned to −40–30 mV, and evoked EPSCs measured every 20 s.

Perfusion of NASPM (20 μM) to block CP-AMPARs or D-2-amino-5-phosphonovaleric acid (D-APV 50 μM; Tocris) and MK801 (10 μM; Tocris) to block NMDARs was initiated

just prior to induction of LTP or LTD and were estimated to be maximal concentrations within ~1 min, when bath exchange was complete (2 × 0.5 mL bath volumes × 1 ml/min flow rate). If the access resistance of any of the above recordings changed by more than 20%, the recording was discarded. Data were collected using pCLAMP and analysed using Mini-Analysis Program and Clampfit.

Golgi staining and dendritic spine counting—Golgi staining of brains was performed as per manufacturer's instructions using FD Rapid GolgiStain Kit (FD Neurotechnologies) as previously described (Sanderson et al., 2012). Briefly, Golgi-stained pyramidal neuron apical dendrites in CA1 in stratum radiatum were imaged by transmitted light on a Zeiss Axiovert 200M microscope, using a 63x Plan-Apo/1.4 NA objective and a Coolsnap CCD camera (Photometrics) operated by Slidebook 5.0 software (Intelligent Imaging Innovations). Spines were counted from image stacks using ImageJ for 20–105 μm segments of secondary or higher-order dendrites > 40 μm from the cell body. Counts are expressed as spines/μm for three mice per genotype with 19 to 21 neurons from different sections along the rostral-caudal axis analyzed per mouse and between one and four dendritic segments counted and averaged per neuron (n = # neurons).

QUANTIFICATION AND STATISTICAL ANALYSIS

fEPSP slope measurements and analyses were made using WinLTP or Scope54. Whole-cell EPSC measurements and analyses were made using in Clampfit (for evoked EPSCs) and Mini Analysis (for sEPSCs). LTP and LTD time-course data were analyzed using standard two-way ANOVA in Prism (GraphPad). Group comparisons where indicated were performed in Prism using one-way ANOVA with Dunnett's correction for multiple comparisons with a control group or Bonferroni correction for multiple comparisons between pairs of groups. Significance is reported as *$p < 0.05$ and data are expressed and graphed as mean ± SEM. In most cases, were possible, the raw data points are also represented on the graphs. For one-way and two-way ANOVA, actual p values are reported in the Results text when provided by the software. When actual p values are not provided by the software only *$p < 0.05$, **$p < 0.01$, **$p < 0.001$, and ****$p < 0.0001$ are reported in the Results text. In addition, only *$p < 0.05$, **$p < 0.01$, **$p < 0.001$, and ****$p < 0.0001$ are reported in the Figure Legends.

Supplementary Material

Refer to Web version on PubMed Central for supplementary material.

ACKNOWLEDGMENTS

This work was supported by NIH grants R01NS040701 and R01NS110383 to M.L.D. and gift funds from the University of Colorado Alzheimer's and Cognition Center provided by Huntington Potter, PhD, Director. The contents are the authors' sole responsibility and do not necessarily represent official NIH views.

REFERENCES

Adesnik H, and Nicoll RA (2007). Conservation of glutamate receptor 2-containing AMPA receptors during long-term potentiation. J. Neurosci 27, 4598–4602. [PubMed: 17460072]

Ancona Esselmann SG, Díaz-Alonso J, Levy JM, Bemben MA, and Nicoll RA (2017). Synaptic homeostasis requires the membrane-proximal carboxy tail of GluA2. Proc. Natl. Acad. Sci. USA 114, 13266–13271. [PubMed: 29180434]

Aoto J, Nam CI, Poon MM, Ting P, and Chen L (2008). Synaptic signaling by all-trans retinoic acid in homeostatic synaptic plasticity. Neuron 60, 308–320. [PubMed: 18957222]

Barcomb K, Hell JW, Benke TA, and Bayer KU (2016). The CaMKII/GluN2B Protein Interaction Maintains Synaptic Strength. J. Biol. Chem 291, 16082–16089. [PubMed: 27246855]

Brachet A, Norwood S, Brouwers JF, Palomer E, Helms JB, Dotti CG, and Esteban JA (2015). LTP-triggered cholesterol redistribution activates Cdc42 and drives AMPA receptor synaptic delivery. J. Cell Biol 208, 791–806. [PubMed: 25753037]

Buonarati OR, Hammes EA, Watson JF, Greger IH, and Hell JW (2019). Mechanisms of postsynaptic localization of AMPA-type glutamate receptors and their regulation during long-term potentiation. Sci. Signal 12.

Chakroborty S, Briggs C, Miller MB, Goussakov I, Schneider C, Kim J, Wicks J, Richardson JC, Conklin V, Cameransi BG, and Stutzmann GE (2012a). Stabilizing ER Ca2+ channel function as an early preventative strategy for Alzheimer's disease. PLoS ONE 7, e52056. [PubMed: 23284867]

Chakroborty S, Kim J, Schneider C, Jacobson C, Molgó J, and Stutzmann GE (2012b). Early presynaptic and postsynaptic calcium signaling abnormalities mask underlying synaptic depression in presymptomatic Alzheimer's disease mice. J. Neurosci 32, 8341–8353. [PubMed: 22699914]

Chen L, Lau AG, and Sarti F (2014). Synaptic retinoic acid signaling and homeostatic synaptic plasticity. Neuropharmacology 78, 3–12. [PubMed: 23270606]

Chen Y, Granger AJ, Tran T, Saulnier JL, Kirkwood A, and Sabatini BL (2017). Endogenous Gαq-Coupled Neuromodulator Receptors Activate Protein Kinase A. Neuron 96, 1070–1083.e5. [PubMed: 29154125]

Choquet D (2018). Linking Nanoscale Dynamics of AMPA Receptor Organization to Plasticity of Excitatory Synapses and Learning. J. Neurosci 38, 9318–9329. [PubMed: 30381423]

Clem RL, and Huganir RL (2010). Calcium-permeable AMPA receptor dynamics mediate fear memory erasure. Science 330, 1108–1112. [PubMed: 21030604]

Collingridge GL, Peineau S, Howland JG, and Wang YT (2010). Longterm depression in the CNS. Nat. Rev. Neurosci 11, 459–473. [PubMed: 20559335]

D'Amelio M, Cavallucci V, Middei S, Marchetti C, Pacioni S, Ferri A, Diamantini A, De Zio D, Carrara P, Battistini L, et al. (2011). Caspase-3 triggers early synaptic dysfunction in a mouse model of Alzheimer's disease. Nat. Neurosci 14, 69–76. [PubMed: 21151119]

Diering GH, and Huganir RL (2018). The AMPA Receptor Code of Synaptic Plasticity. Neuron 100, 314–329. [PubMed: 30359599]

Diering GH, Gustina AS, and Huganir RL (2014). PKA-GluA1 coupling via AKAP5 controls AMPA receptor phosphorylation and cell-surface targeting during bidirectional homeostatic plasticity. Neuron 84, 790–805. [PubMed: 25451194]

Dineley KT, Hogan D, Zhang WR, and Taglialatela G (2007). Acute inhibition of calcineurin restores associative learning and memory in Tg2576 APP transgenic mice. Neurobiol. Learn. Mem 88, 217–224. [PubMed: 17521929]

Dineley KT, Kayed R, Neugebauer V, Fu Y, Zhang W, Reese LC, and Taglialatela G (2010). Amyloid-beta oligomers impair fear conditioned memory in a calcineurin-dependent fashion in mice. J. Neurosci. Res 88, 2923–2932. [PubMed: 20544830]

Efendiev R, Samelson BK, Nguyen BT, Phatarpekar PV, Baameur F, Scott JD, and Dessauer CW (2010). AKAP79 interacts with multiple adenylyl cyclase (AC) isoforms and scaffolds AC5 and −6 to alpha-amino-3-hydroxyl-5-methyl-4-isoxazole-propionate (AMPA) receptors. J. Biol. Chem 285, 14450–14458. [PubMed: 20231277]

Esteban JA, Shi S-H, Wilson C, Nuriya M, Huganir RL, and Malinow R (2003). PKA phosphorylation of AMPA receptor subunits controls synaptic trafficking underlying plasticity. Nat. Neurosci 6, 136–143. [PubMed: 12536214]

Freund RK, Gibson ES, Potter H, and Dell'Acqua ML (2016). Inhibition of the Motor Protein Eg5/Kinesin-5 in Amyloid β-Mediated Impairment of Hippocampal Long-Term Potentiation and Dendritic Spine Loss. Mol. Pharmacol 89, 552–559. [PubMed: 26957206]

Goel A, Xu LW, Snyder KP, Song L, Goenaga-Vazquez Y, Megill A, Takamiya K, Huganir RL, and Lee HK (2011). Phosphorylation of AMPA receptors is required for sensory deprivation-induced homeostatic synaptic plasticity. PLoS ONE 6, e18264. [PubMed: 21483826]

Goodell DJ, Zaegel V, Coultrap SJ, Hell JW, and Bayer KU (2017). DAPK1 Mediates LTD by Making CaMKII/GluN2B Binding LTP Specific. Cell Rep. 19, 2231–2243. [PubMed: 28614711]

Goussakov I, Miller MB, and Stutzmann GE (2010). NMDA-mediated Ca(2+) influx drives aberrant ryanodine receptor activation in dendrites of young Alzheimer's disease mice. J. Neurosci 30, 12128–12137. [PubMed: 20826675]

Granger AJ, Shi Y, Lu W, Cerpas M, and Nicoll RA (2013). LTP requires a reserve pool of glutamate receptors independent of subunit type. Nature 493, 495–500. [PubMed: 23235828]

Gray EE, Fink AE, Sariñana J, Vissel B, and O'Dell TJ (2007). Longterm potentiation in the hippocampal CA1 region does not require insertion and activation of GluR2-lacking AMPA receptors. J. Neurophysiol 98, 2488–2492. [PubMed: 17652419]

Guire ES, Oh MC, Soderling TR, and Derkach VA (2008). Recruitment of calcium-permeable AMPA receptors during synaptic potentiation is regulated by CaM-kinase I. J. Neurosci 28, 6000–6009. [PubMed: 18524905]

Haas LT, and Strittmatter SM (2016). Oligomers of Amyloid β Prevent Physiological Activation of the Cellular Prion Protein-Metabotropic Glutamate Receptor 5 Complex by Glutamate in Alzheimer Disease. J. Biol. Chem 291, 17112–17121. [PubMed: 27325698]

Haas LT, Kostylev MA, and Strittmatter SM (2014). Therapeutic molecules and endogenous ligands regulate the interaction between brain cellular prion protein (PrPC) and metabotropic glutamate receptor 5 (mGluR5). J. Biol. Chem 289, 28460–28477. [PubMed: 25148681]

Halt AR, Dallapiazza RF, Zhou Y, Stein IS, Qian H, Juntti S, Wojcik S, Brose N, Silva AJ, and Hell JW (2012). CaMKII binding to GluN2B is critical during memory consolidation. EMBO J. 31, 1203–1216. [PubMed: 22234183]

He K, Song L, Cummings LW, Goldman J, Huganir RL, and Lee HK (2009). Stabilization of Ca2+-permeable AMPA receptors at perisynaptic sites by GluR1-S845 phosphorylation. Proc. Natl. Acad. Sci. USA 106, 20033–20038. [PubMed: 19892736]

Herring BE, and Nicoll RA (2016). Kalirin and Trio proteins serve critical roles in excitatory synaptic transmission and LTP. Proc. Natl. Acad. Sci. USA 113, 2264–2269. [PubMed: 26858404]

Hsieh H, Boehm J, Sato C, Iwatsubo T, Tomita T, Sisodia S, and Malinow R (2006). AMPAR removal underlies Abeta-induced synaptic depression and dendritic spine loss. Neuron 52, 831–843. [PubMed: 17145504]

Huganir RL, and Nicoll RA (2013). AMPARs and synaptic plasticity: the last 25 years. Neuron 80, 704–717. [PubMed: 24183021]

Jensen V, Kaiser KM, Borchardt T, Adelmann G, Rozov A, Burnashev N, Brix C, Frotscher M, Andersen P, Hvalby Ø, et al. (2003). A juvenile form of postsynaptic hippocampal long-term potentiation in mice deficient for the AMPA receptor subunit GluR-A. J. Physiol 553, 843–856. [PubMed: 14555717]

Jo J, Whitcomb DJ, Olsen KM, Kerrigan TL, Lo SC, Bru-Mercier G, Dickinson B, Scullion S, Sheng M, Collingridge G, and Cho K (2011). Aβ(1–42) inhibition of LTP is mediated by a signaling pathway involving caspase-3, Akt1 and GSK-3β. Nat. Neurosci 14, 545–547. [PubMed: 21441921]

Keith DJ, Sanderson JL, Gibson ES, Woolfrey KM, Robertson HR, Olszewski K, Kang R, El-Husseini A, and Dell'acqua ML (2012). Palmitoylation of A-kinase anchoring protein 79/150 regulates dendritic endosomal targeting and synaptic plasticity mechanisms. J. Neurosci 32, 7119–7136. [PubMed: 22623657]

Kennedy MJ, Davison IG, Robinson CG, and Ehlers MD (2010). Syntaxin-4 defines a domain for activity-dependent exocytosis in dendritic spines. Cell 141, 524–535. [PubMed: 20434989]

Kim S, and Ziff EB (2014). Calcineurin mediates synaptic scaling via synaptic trafficking of Ca2+-permeable AMPA receptors. PLoS Biol. 12, e1001900. [PubMed: 24983627]

Kim S, Violette CJ, and Ziff EB (2015). Reduction of increased calcineurin activity rescues impaired homeostatic synaptic plasticity in presenilin 1 M146V mutant. Neurobiol. Aging 36, 3239–3246. [PubMed: 26455952]

Kolleker A, Zhu JJ, Schupp BJ, Qin Y, Mack V, Borchardt T, Köhr G, Malinow R, Seeburg PH, and Osten P (2003). Glutamatergic plasticity by synaptic delivery of GluR-B(long)-containing AMPA receptors. Neuron 40, 1199–1212. [PubMed: 14687553]

Lee HK, Takamiya K, Han JS, Man H, Kim CH, Rumbaugh G, Yu S, Ding L, He C, Petralia RS, et al. (2003). Phosphorylation of the AMPA receptor GluR1 subunit is required for synaptic plasticity and retention of spatial memory. Cell 112, 631–643. [PubMed: 12628184]

Lee HK, Takamiya K, He K, Song L, and Huganir RL (2010). Specific roles of AMPA receptor subunit GluR1 (GluA1) phosphorylation sites in regulating synaptic plasticity in the CA1 region of hippocampus. J. Neurophysiol 103, 479–489. [PubMed: 19906877]

Lee KF, Soares C, and Béïque JC (2013). Tuning into diversity of homeostatic synaptic plasticity. Neuropharmacology 78, 31–37. [PubMed: 23541721]

Li S, Jin M, Koeglsperger T, Shepardson NE, Shankar GM, and Selkoe DJ (2011). Soluble Aβ oligomers inhibit long-term potentiation through a mechanism involving excessive activation of extrasynaptic NR2B-containing NMDA receptors. J. Neurosci 31, 6627–6638. [PubMed: 21543591]

Li S, Jin M, Zhang D, Yang T, Koeglsperger T, Fu H, and Selkoe DJ (2013). Environmental novelty activates β2-adrenergic signaling to prevent the impairment of hippocampal LTP by Aβ oligomers. Neuron 77, 929–941. [PubMed: 23473322]

Lu Y, Allen M, Halt AR, Weisenhaus M, Dallapiazza RF, Hall DD, Usachev YM, McKnight GS, and Hell JW (2007). Age-dependent requirement of AKAP150-anchored PKA and GluR2-lacking AMPA receptors in LTP. EMBO J. 26, 4879–4890. [PubMed: 17972919]

Lu W, Shi Y, Jackson AC, Bjorgan K, During MJ, Sprengel R, Seeburg PH, and Nicoll RA (2009). Subunit composition of synaptic AMPA receptors revealed by a single-cell genetic approach. Neuron 62, 254–268. [PubMed: 19409270]

Lu Y, Zha XM, Kim EY, Schachtele S, Dailey ME, Hall DD, Strack S, Green SH, Hoffman DA, and Hell JW (2011). A kinase anchor protein 150 (AKAP150)-associated protein kinase A limits dendritic spine density. J. Biol. Chem 286, 26496–26506. [PubMed: 21652711]

Murphy JG, Sanderson JL, Gorski JA, Scott JD, Catterall WA, Sather WA, and Dell'Acqua ML (2014). AKAP-anchored PKA maintains neuronal L-type calcium channel activity and NFAT transcriptional signaling. Cell Rep. 7, 1577–1588. [PubMed: 24835999]

Nair D, Hosy E, Petersen JD, Constals A, Giannone G, Choquet D, and Sibarita JB (2013). Super-resolution imaging reveals that AMPA receptors inside synapses are dynamically organized in nanodomains regulated by PSD95. J. Neurosci 33, 13204–13224. [PubMed: 23926273]

Opazo P, Labrecque S, Tigaret CM, Frouin A, Wiseman PW, De Koninck P, and Choquet D (2010). CaMKII triggers the diffusional trapping of surface AMPARs through phosphorylation of stargazin. Neuron 67, 239–252. [PubMed: 20670832]

Opazo P, Sainlos M, and Choquet D (2012). Regulation of AMPA receptor surface diffusion by PSD-95 slots. Curr. Opin. Neurobiol 22, 453–460. [PubMed: 22051694]

Park M, Penick EC, Edwards JG, Kauer JA, and Ehlers MD (2004). Recycling endosomes supply AMPA receptors for LTP. Science 305, 1972–1975. [PubMed: 15448273]

Park P, Sanderson TM, Amici M, Choi SL, Bortolotto ZA, Zhuo M, Kaang BK, and Collingridge GL (2016). Calcium-Permeable AMPA Receptors Mediate the Induction of the Protein Kinase A-Dependent Component of Long-Term Potentiation in the Hippocampus. J. Neurosci 36, 622–631. [PubMed: 26758849]

Park P, Georgiou J, Sanderson TM, Ko KH, Kang H, Kim JI, Bradley CA, Bortolotto ZA, Zhuo M, Kaang BK, and Collingridge GL (2021). PKA drives an increase in AMPA receptor unitary conductance during LTP in the hippocampus. Nat. Commun 12, 413. [PubMed: 33462202]

Penn AC, Zhang CL, Georges F, Royer L, Breillat C, Hosy E, Petersen JD, Humeau Y, and Choquet D (2017). Hippocampal LTP and contextual learning require surface diffusion of AMPA receptors. Nature 549, 384–388. [PubMed: 28902836]

Petrini EM, Lu J, Cognet L, Lounis B, Ehlers MD, and Choquet D (2009). Endocytic trafficking and recycling maintain a pool of mobile surface AMPA receptors required for synaptic potentiation. Neuron 63, 92–105. [PubMed: 19607795]

Plant K, Pelkey KA, Bortolotto ZA, Morita D, Terashima A, McBain CJ, Collingridge GL, and Isaac JT (2006). Transient incorporation of native GluR2-lacking AMPA receptors during hippocampal long-term potentiation. Nat. Neurosci 9, 602–604. [PubMed: 16582904]

Popugaeva E, Pchitskaya E, and Bezprozvanny I (2017). Dysregulation of neuronal calcium homeostasis in Alzheimer's disease - A therapeutic opportunity? Biochem. Biophys. Res. Commun 483, 998–1004. [PubMed: 27641664]

Purkey AM, and Dell'Acqua ML (2020). Phosphorylation-Dependent Regulation of Ca^{2+}-Permeable AMPA Receptors During Hippocampal Synaptic Plasticity. Front. Synaptic Neurosci 12, 8. [PubMed: 32292336]

Purkey AM, Woolfrey KM, Crosby KC, Stich DG, Chick WS, Aoto J, and Dell'Acqua ML (2018). AKAP150 Palmitoylation Regulates Synaptic Incorporation of Ca^{2+}-Permeable AMPA Receptors to Control LTP. Cell Rep. 25, 974–987.e4. [PubMed: 30355502]

Reese LC, Zhang W, Dineley KT, Kayed R, and Taglialatela G (2008). Selective induction of calcineurin activity and signaling by oligomeric amyloid beta. Aging Cell 7, 824–835. [PubMed: 18782350]

Rozov A, Sprengel R, and Seeburg PH (2012). GluA2-lacking AMPA receptors in hippocampal CA1 cell synapses: evidence from gene-targeted mice. Front. Mol. Neurosci 5, 22. [PubMed: 22375105]

Sanderson JL, Gorski JA, Gibson ES, Lam P, Freund RK, Chick WS, and Dell'Acqua ML (2012). AKAP150-anchored calcineurin regulates synaptic plasticity by limiting synaptic incorporation of Ca2+-permeable AMPA receptors. J. Neurosci 32, 15036–15052. [PubMed: 23100425]

Sanderson JL, Gorski JA, and Dell'Acqua ML (2016). NMDA Receptor-Dependent LTD Requires Transient Synaptic Incorporation of Ca^{2+}-Permeable AMPARs Mediated by AKAP150-Anchored PKA and Calcineurin. Neuron 89, 1000–1015. [PubMed: 26938443]

Sanderson JL, Scott JD, and Dell'Acqua ML (2018). Control of Homeostatic Synaptic Plasticity by AKAP-Anchored Kinase and Phosphatase Regulation of Ca^{2+}-Permeable AMPA Receptors. J. Neurosci 38, 2863–2876. [PubMed: 29440558]

Sanhueza M, Fernandez-Villalobos G, Stein IS, Kasumova G, Zhang P, Bayer KU, Otmakhov N, Hell JW, and Lisman J (2011). Role of the CaM-KII/NMDA receptor complex in the maintenance of synaptic strength. J. Neurosci 31, 9170–9178. [PubMed: 21697368]

Shankar GM, Bloodgood BL, Townsend M, Walsh DM, Selkoe DJ, and Sabatini BL (2007). Natural oligomers of the Alzheimer amyloid-beta protein induce reversible synapse loss by modulating an NMDA-type glutamate receptor-dependent signaling pathway. J. Neurosci 27, 2866–2875. [PubMed: 17360908]

Shankar GM, Li S, Mehta TH, Garcia-Munoz A, Shepardson NE, Smith I, Brett FM, Farrell MA, Rowan MJ, Lemere CA, et al. (2008). Amyloid-beta protein dimers isolated directly from Alzheimer's brains impair synaptic plasticity and memory. Nat. Med 14, 837–842. [PubMed: 18568035]

Sinnen BL, Bowen AB, Gibson ES, and Kennedy MJ (2016). Local and Use-Dependent Effects of β-Amyloid Oligomers on NMDA Receptor Function Revealed by Optical Quantal Analysis. J. Neurosci 36, 11532–11543. [PubMed: 27911757]

Sinnen BL, Bowen AB, Forte JS, Hiester BG, Crosby KC, Gibson ES, Dell'Acqua ML, and Kennedy MJ (2017). Optogenetic Control of Synaptic Composition and Function. Neuron 93, 646–660.e5. [PubMed: 28132827]

Soares C, Lee KF, Nassrallah W, and Béïque JC (2013). Differential subcellular targeting of glutamate receptor subtypes during homeostatic synaptic plasticity. J. Neurosci 33, 13547–13559. [PubMed: 23946413]

Steele PM, and Mauk MD (1999). Inhibitory control of LTP and LTD: stability of synapse strength. J. Neurophysiol 81, 1559–1566. [PubMed: 10200191]

Stubblefield EA, and Benke TA (2010). Distinct AMPA-type glutamatergic synapses in developing rat CA1 hippocampus. J. Neurophysiol 104, 1899–1912. [PubMed: 20685930]

Sutton MA, Ito HT, Cressy P, Kempf C, Woo JC, and Schuman EM (2006). Miniature neurotransmission stabilizes synaptic function via tonic suppression of local dendritic protein synthesis. Cell 125, 785–799. [PubMed: 16713568]

Taglialatela G, Hogan D, Zhang WR, and Dineley KT (2009). Intermediate- and long-term recognition memory deficits in Tg2576 mice are reversed with acute calcineurin inhibition. Behav. Brain Res 200, 95–99. [PubMed: 19162087]

Taglialatela G, Rastellini C, and Cicalese L (2015). Reduced Incidence of Dementia in Solid Organ Transplant Patients Treated with Calcineurin Inhibitors. J. Alzheimers Dis 47, 329–333. [PubMed: 26401556]

Tang AH, Chen H, Li TP, Metzbower SR, MacGillavry HD, and Blanpied TA (2016). A trans-synaptic nanocolumn aligns neurotransmitter release to receptors. Nature 536, 210–214. [PubMed: 27462810]

Thiagarajan TC, Lindskog M, and Tsien RW (2005). Adaptation to synaptic inactivity in hippocampal neurons. Neuron 47, 725–737. [PubMed: 16129401]

Traynelis SF, Wollmuth LP, McBain CJ, Menniti FS, Vance KM, Ogden KK, Hansen KB, Yuan H, Myers SJ, and Dingledine R (2010). Glutamate receptor ion channels: structure, regulation, and function. Pharmacol. Rev 62, 405–496. [PubMed: 20716669]

Turrigiano G (2012). Homeostatic synaptic plasticity: local and global mechanisms for stabilizing neuronal function. Cold Spring Harb. Perspect. Biol 4, a005736. [PubMed: 22086977]

Vitolo OV, Sant'Angelo A, Costanzo V, Battaglia F, Arancio O, and Shelanski M (2002). Amyloid beta -peptide inhibition of the PKA/CREB pathway and long-term potentiation: reversibility by drugs that enhance cAMP signaling. Proc. Natl. Acad. Sci. USA 99, 13217–13221. [PubMed: 12244210]

Wang Q, Walsh DM, Rowan MJ, Selkoe DJ, and Anwyl R (2004). Block of long-term potentiation by naturally secreted and synthetic amyloid beta-peptide in hippocampal slices is mediated via activation of the kinases c-Jun N-terminal kinase, cyclin-dependent kinase 5, and p38 mitogen-activated protein kinase as well as metabotropic glutamate receptor type 5. J. Neurosci 24, 3370–3378. [PubMed: 15056716]

Wang QW, Rowan MJ, and Anwyl R (2009). Inhibition of LTP by beta-amyloid is prevented by activation of beta2 adrenoceptors and stimulation of the cAMP/PKA signalling pathway. Neurobiol. Aging 30, 1608–1613. [PubMed: 18272254]

Wang D, Fu Q, Zhou Y, Xu B, Shi Q, Igwe B, Matt L, Hell JW, Wisely EV, Oddo S, and Xiang YK (2013). β2 adrenergic receptor, protein kinase A (PKA) and c-Jun N-terminal kinase (JNK) signaling pathways mediate tau pathology in Alzheimer disease models. J. Biol. Chem 288, 10298–10307. [PubMed: 23430246]

Whitcomb DJ, Hogg EL, Regan P, Piers T, Narayan P, Whitehead G, Winters BL, Kim DH, Kim E, St George-Hyslop P, et al. (2015). Intracellular oligomeric amyloid-beta rapidly regulates GluA1 subunit of AMPA receptor in the hippocampus. Sci. Rep 5, 10934. [PubMed: 26055072]

Willoughby D, Masada N, Wachten S, Pagano M, Halls ML, Everett KL, Ciruela A, and Cooper DM (2010). AKAP79/150 interacts with AC8 and regulates Ca2+-dependent cAMP synthesis in pancreatic and neuronal systems. J. Biol. Chem 285, 20328–20342. [PubMed: 20410303]

Wolf ME, and Tseng KY (2012). Calcium-permeable AMPA receptors in the VTA and nucleus accumbens after cocaine exposure: when, how, and why? Front. Mol. Neurosci 5, 72. [PubMed: 22754497]

Woolfrey KM, Sanderson JL, and Dell'Acqua ML (2015). The palmitoyl acyltransferase DHHC2 regulates recycling endosome exocytosis and synaptic potentiation through palmitoylation of AKAP79/150. J. Neurosci 35, 442–456. [PubMed: 25589740]

Wu HY, Hudry E, Hashimoto T, Kuchibhotla K, Rozkalne A, Fan Z, Spires-Jones T, Xie H, Arbel-Ornath M, Grosskreutz CL, et al. (2010). Amyloid beta induces the morphological neurodegenerative triad of spine loss, dendritic simplification, and neuritic dystrophies through calcineurin activation. J. Neurosci 30, 2636–2649. [PubMed: 20164348]

Yamin G (2009). NMDA receptor-dependent signaling pathways that underlie amyloid beta-protein disruption of LTP in the hippocampus. J. Neurosci. Res 87, 1729–1736. [PubMed: 19170166]

Yang Y, Wang XB, and Zhou Q (2010). Perisynaptic GluR2-lacking AMPA receptors control the reversibility of synaptic and spines modifications. Proc. Natl. Acad. Sci. USA 107, 11999–12004. [PubMed: 20547835]

Zamanillo D, Sprengel R, Hvalby O, Jensen V, Burnashev N, Rozov A, Kaiser KM, Köster HJ, Borchardt T, Worley P, et al. (1999). Importance of AMPA receptors for hippocampal synaptic plasticity but not for spatial learning. Science 284, 1805–1811. [PubMed: 10364547]

Zhao WQ, Santini F, Breese R, Ross D, Zhang XD, Stone DJ, Ferrer M, Townsend M, Wolfe AL, Seager MA, et al. (2010). Inhibition of calcineurin-mediated endocytosis and alpha-amino-3-hydroxy-5-methyl-4-isoxa-zolepropionic acid (AMPA) receptors prevents amyloid beta oligomer-induced synaptic disruption. J. Biol. Chem 285, 7619–7632. [PubMed: 20032460]

Zhou Z, Liu A, Xia S, Leung C, Qi J, Meng Y, Xie W, Park P, Collingridge GL, and Jia Z (2018). The C-terminal tails of endogenous GluA1 and GluA2 differentially contribute to hippocampal synaptic plasticity and learning. Nat. Neurosci 21, 50–62. [PubMed: 29230056]

Highlights

- Anchored PKA and CaN exert opposing control of CP-AMPARs at adult CA1 synapses
- AKAP-PKA signaling recruits CP-AMPARs during LTP, LTD and following Aβ exposure
- CP-AMPARs prime synapses for LTD and Aβ inhibition of LTP mediated by AKAP-CaN
- Aβ hijacks CP-AMPAR regulation by PKA/CaN to tip LTP/LTD balance in favor of LTD

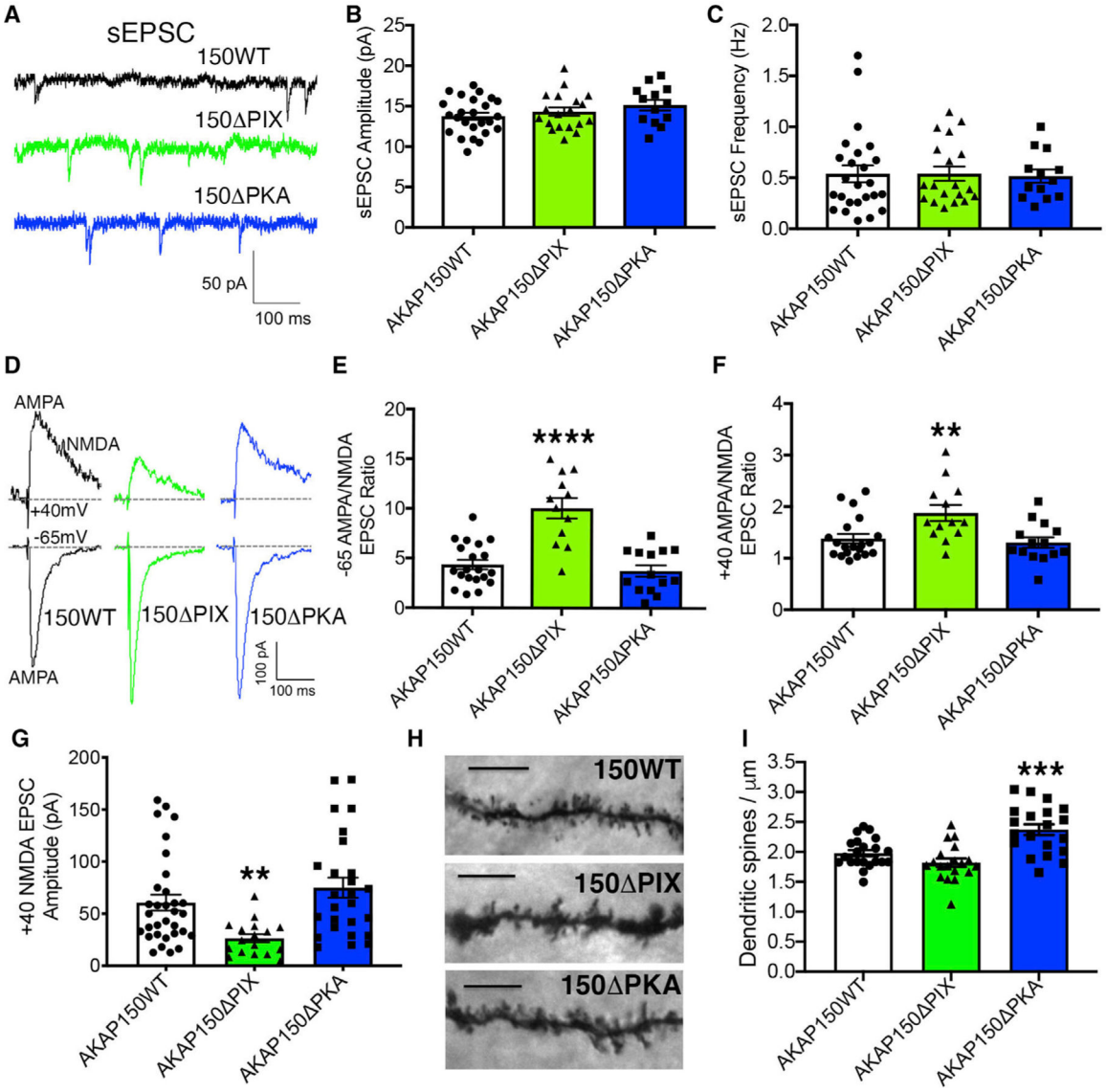

Figure 1. Characterization of basal excitatory synaptic transmission in hippocampal area CA1 in adult PKA anchoring-deficient 150ΔPKA and CaN anchoring-deficient 150ΔPIX mice

(A–C) Representative recordings from CA1 pyramidal neurons (A) and quantification of mean sEPSC amplitude (WT 13.8 ± 0.5 pA, n = 25; 150ΔPIX 14.3 ± 0.6 pA, n = 19; 150ΔPKA 15.1 ± 0.7 pA, n = 13) (B) and frequency (WT 0.54 ± 0.08 Hz, n = 25; 150ΔPIX 0.54 ± 0.07 Hz, n = 19; 150ΔPKA 0.52 ± 0.07 Hz, n = 13) (C).

(D) Representative recordings of evoked SC-CA1 −65 mV inward AMPA and +40 mV outward mixed AMPA and NMDA EPSCs.

(E–G) Quantification of mean −65 mV inward AMPA/+40 mV outward NMDA ratio (WT 4.4 ± 0.5, n = 20; 150ΔPIX 10 ± 1, n = 12, ****p < 0.0001 by one-way ANOVA with Dunnett's; 150ΔPKA 3.8 ± 0.6, n = 14) (E), +40 outward AMPA/+40 mV outward NMDA EPSC ratio (WT 1.4 ± 0.1, n = 21; 150ΔPIX 1.9 ± 0.2, n = 13, **p < 0.01 by one-way ANOVA with Dunnett's; 150ΔPKA 1.4 ± 0.2, n = 15) (F), and +40 mV outward NMDA EPSC amplitude measured 70 ms after the onset of the response (WT 61 ± 8 pA, n = 32;

150ΔPIX 27 ± 4 pA, n = 17, **p < 0.01 by one-way ANOVA with Dunnett's; 150ΔPKA 75 ± 10 pA, n = 26) (G).

(H) Imaging of Golgi-stained dendritic segments in the CA1 *stratum radiatum* (scale bars, 5 μm).

(I) Quantification of dendritic spines/μm for WT (1.98 ± 0.05, n = 21), 150ΔPIX (1.82 ± 0.07, n = 19), and 150ΔPKA (2.37 ± 0.09, n = 20, ***p < 0.001 to WT one-way ANOVA with Dunnett's).

All data are represented as mean ± SEM.

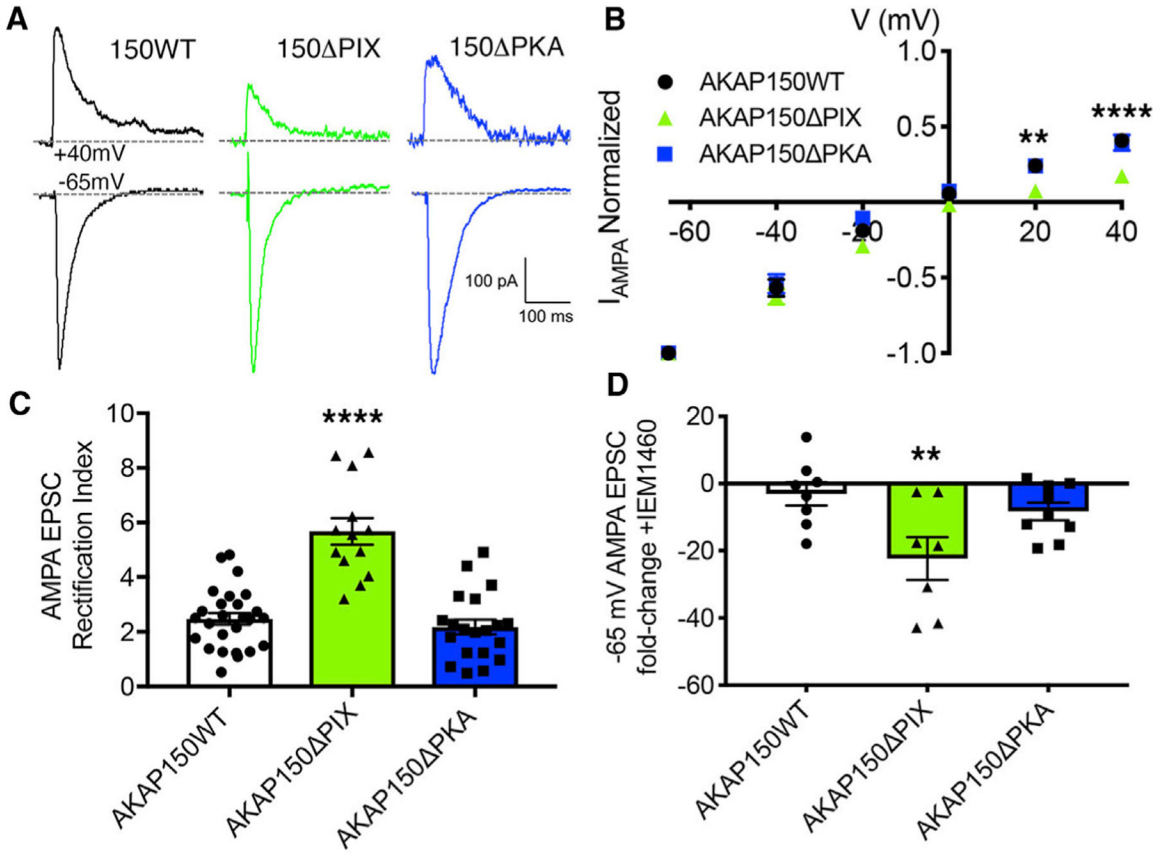

Figure 2. AKAP150-CaN anchoring limits basal synaptic incorporation of CP-AMPARs at SC-CA1 synapses in adult mice

(A and B) Representative recordings of evoked SC-CA1 AMPAR EPSC responses (A) and normalized (to −65 mV response) current amplitudes for a range membrane holding potentials plotted as I-V curves (WT n = 27; 150ΔPKA n = 13; 150ΔPIX n = 14, +20 mV **p < 0.01, +40 mV ****p < 0.0001 by 2-way ANOVA with Bonferroni) (B).

(C) AMPA EPSC −65 mv/+40 mV rectification index calculated from cells recorded in (B) (WT 2.5 ± 0.3, n = 26; 150ΔPKA 2.2 ± 0.3, n = 13; 150ΔPIX 5.7 ± 0.5, n = 13, ****p < 0.0001 by one-way ANOVA with Dunnett's).

(D) Percent change in −65 mV EPSC response after application of the CP-AMPAR antagonist IEM (WT −3.0 ± 3, n = 8; 150ΔPKA −8 ± 3, n = 13; 150ΔPIX −22 ± 6, n = 7, **p < 0.01 by one-way ANOVA with Dunnett's).

All data are represented as mean ± SEM.

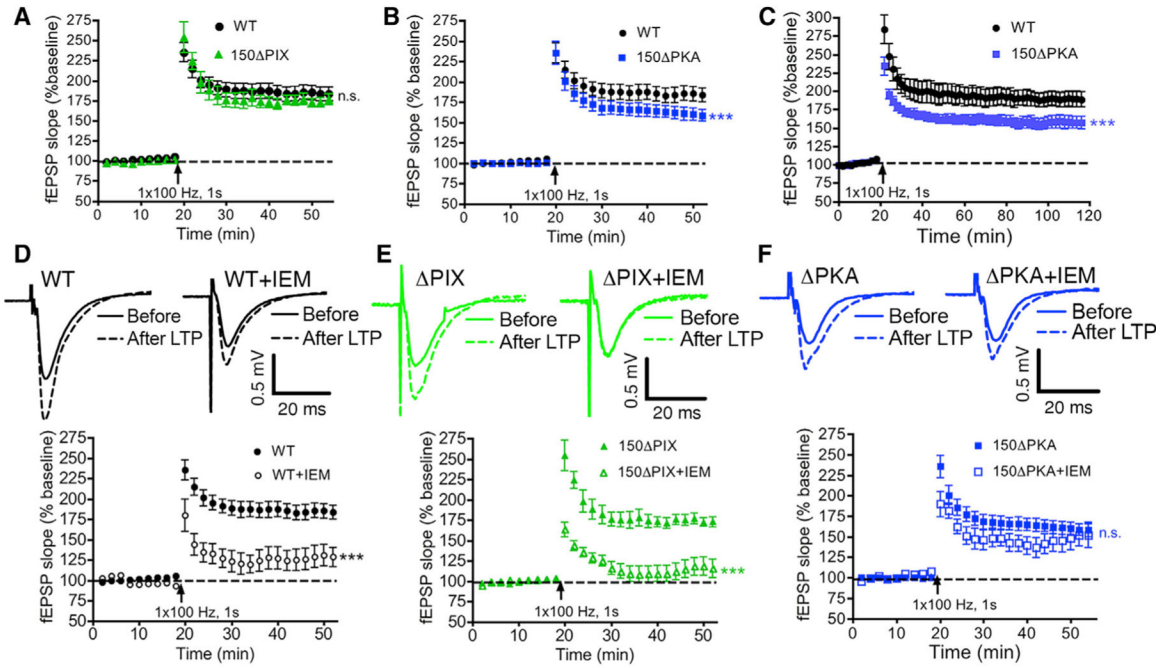

Figure 3. Disruption of AKAP150-PKA anchoring leads to a shift away from CP-AMPAR-dependent expression of 100-Hz LTP at SC-CA1 synapses in adult mice

(A and B) fEPSP slope plotted over time showing that 1 × 100-Hz HFS induces similar levels of LTP expression in 150ΔPIX mice (n = 11, p = 0.097) (A) but reduced LTP expression in 150ΔPKA mice (n = 11, ***p < 0.001 by 2-way ANOVA) (B) compared with WT controls (n = 13).

(C) Expression of 1 × 100-Hz LTP is reduced persistently even at later time points more than 90 min after induction in 150ΔPKA compared with WT mice (WT n = 7, 150ΔPKA n = 8, ***p < 0.001 by 2-way ANOVA).

(D–F) Application of the CP-AMPAR antagonist immediately after 1 × 100-Hz HFS induction significantly inhibits LTP expression in adult WT (n = 13, +IEM n = 5, ***p < 0.001 by 2-way ANOVA) (D) and 150ΔPIX mice (n = 11, +IEM n = 20, ***p < 0.001 by 2-way ANOVA) (E) but not 150ΔPKA mice (n = 11, +IEM n = 8, p = 0.085)

(F). Top panels: representative fEPSP recordings before and 30 min after LTP induction. Bottom panels: fEPSP slope plotted over time. n.s. = not significant. All data are represented as mean ± SEM.

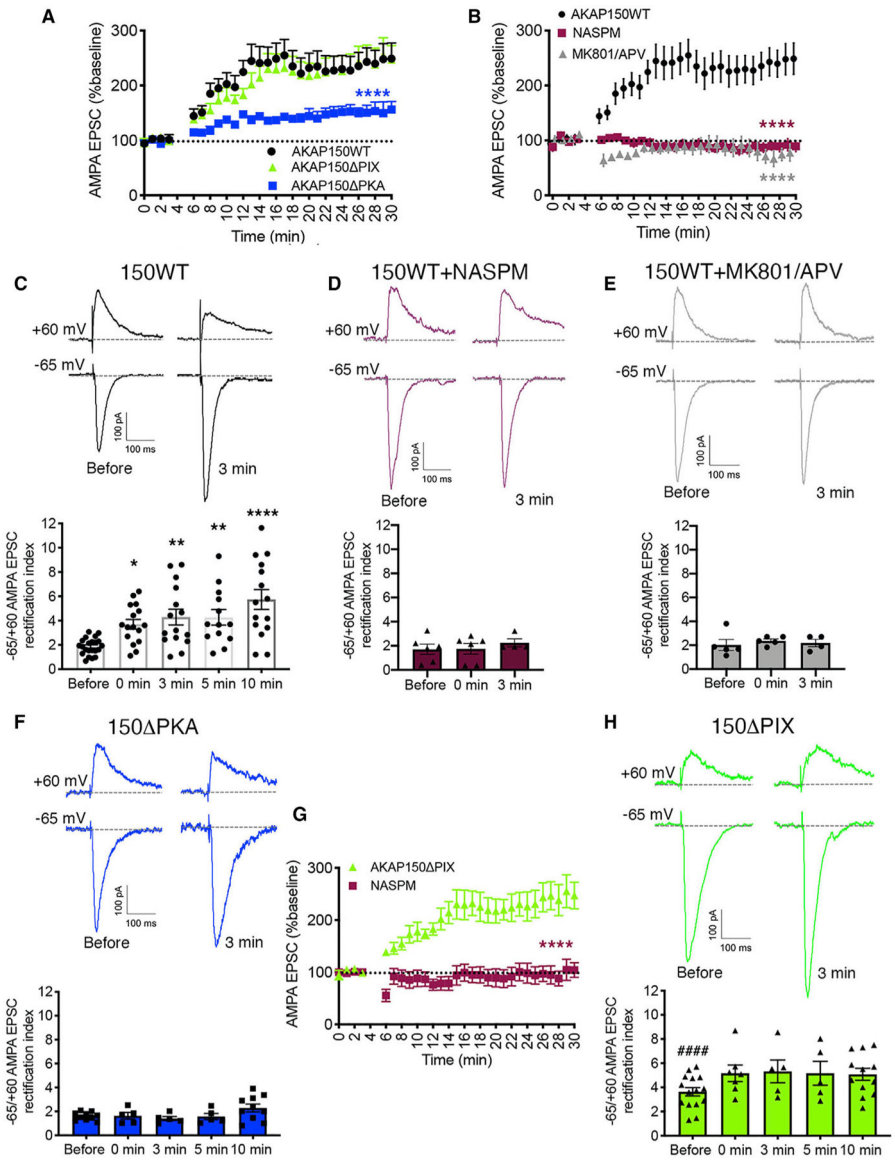

Figure 4. AKAP150-PKA anchoring promotes synaptic recruitment of inwardly rectifying CP-AMPARs to support SC-CA1 LTP expression

(A) LTP of −65 mV AMPA EPSCs at SC-CA1 synapses induced using a whole-cell pairing protocol (3 Hz, 0 mV, picrotoxin) in WT (n = 8), 150ΔPIX (n = 6), and 150ΔPKA mice (n = 4). LTP expression is reduced significantly in 150ΔPKA mice (****p < 0.0001 by 2-way ANOVA and one-way ANOVA with Bonferroni's).

(B) Inhibition of 3-Hz pairing LTP in WT mice by NMDAR (MK801/APV, n = 12, ****p < 0.0001 by 2-way ANOVA and one-way ANOVA with Bonferroni's) and CP-AMPAR antagonism (NASPM n = 7, ****p < 0.0001 by 2-way ANOVA).

(C) 3-Hz pairing LTP increases AMPAR rectification from 0–10 min after induction in WT mice. Top: representative traces. Bottom: graph of the −65 mV/+60 mV AMPA EPSC rectification index (n = 13–22; *p < 0.05, **p < 0.01, ****p < 0.0001 by Dunnett's).

(D and E) 3-Hz pairing stimulation does not increase the AMPAR rectification index in WT mice in the presence of NASPM (D, n = 4–6) or MK801/APV (E, n = 4–5).

(F) 3-Hz pairing stimulation does not increase the AMPAR rectification index in 150ΔPKA mice (n = 5–10). Top: representative traces. Bottom: graph of the −65 mV/+60 mV AMPA EPSC rectification index.

(G) Inhibition of 3-Hz pairing LTP in 150ΔPIX mice by CP-AMPAR antagonism (NASPM n = 9, ****p < 0.0001 by 2-way ANOVA).

(H) −65 mV/+60 mV AMPA EPSC inward rectification compared with the WT is already increased basally in 150ΔPIX mice and remains elevated similarly after 3-Hz LTP induction. Top: representative traces. Bottom: graph of the −65 mV/+60 mV AMPA EPSC rectification index (n = 5–15; ###p < 0.0001 to WT Before by one-way ANOVA with Dunnett's).

All data are represented as mean ± SEM.

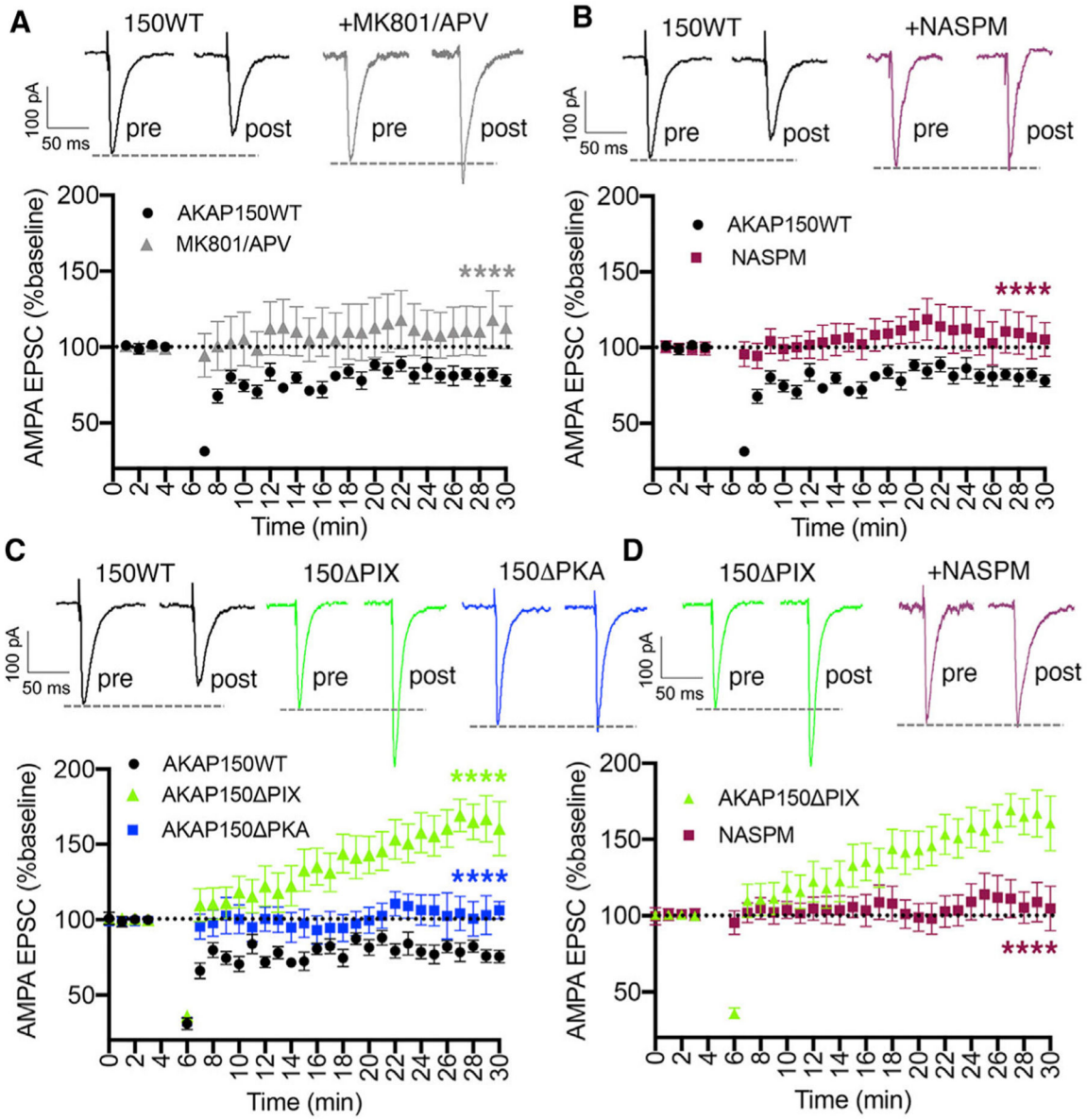

Figure 5. AKAP150-PKA and CaN anchoring are required for CP-AMPAR-dependent LTD at SC-CA1 synapses in adult mice

(A and B) 3-Hz, 0-mV pairing-induced LTD of AMPA EPSCs recorded in the absence of picrotoxin at the Cl^- reversal potential (−30–40 mV) in WT mice (n = 14) is inhibited by antagonists of NMDARs (MK801/APV n = 10, ****p < 0.0001 by 2-way ANOVA and one-way ANOVA) (A) and CP-AMPARs (NASPM n = 11, ****p < 0.0001 by 2-way ANOVA and one-way ANOVA with Bonferroni's)

(B). Top: representative traces.

(C and D) 3-Hz, 0-mV pairing-induced LTD is absent in 150ΔPKA mice (n = 13, compared with WT n = 12, ****p < 0.0001 by 2-way ANOVA and one-way ANOVA with Bonferroni's) and results in inappropriate LTP in 150ΔPIX mice (n = 14, compared with WT n = 12, ****p < 0.0001 by 2-way ANOVA and one-way ANOVA with Bonferroni's) (C),

which is prevented by antagonism of CP-AMPAR (NASPM n = 9, ****p < 0.0001 by 2-way ANOVA and one-way ANOVA with Bonferroni's) (D). Top: representative traces.
All data are represented as mean ± SEM.

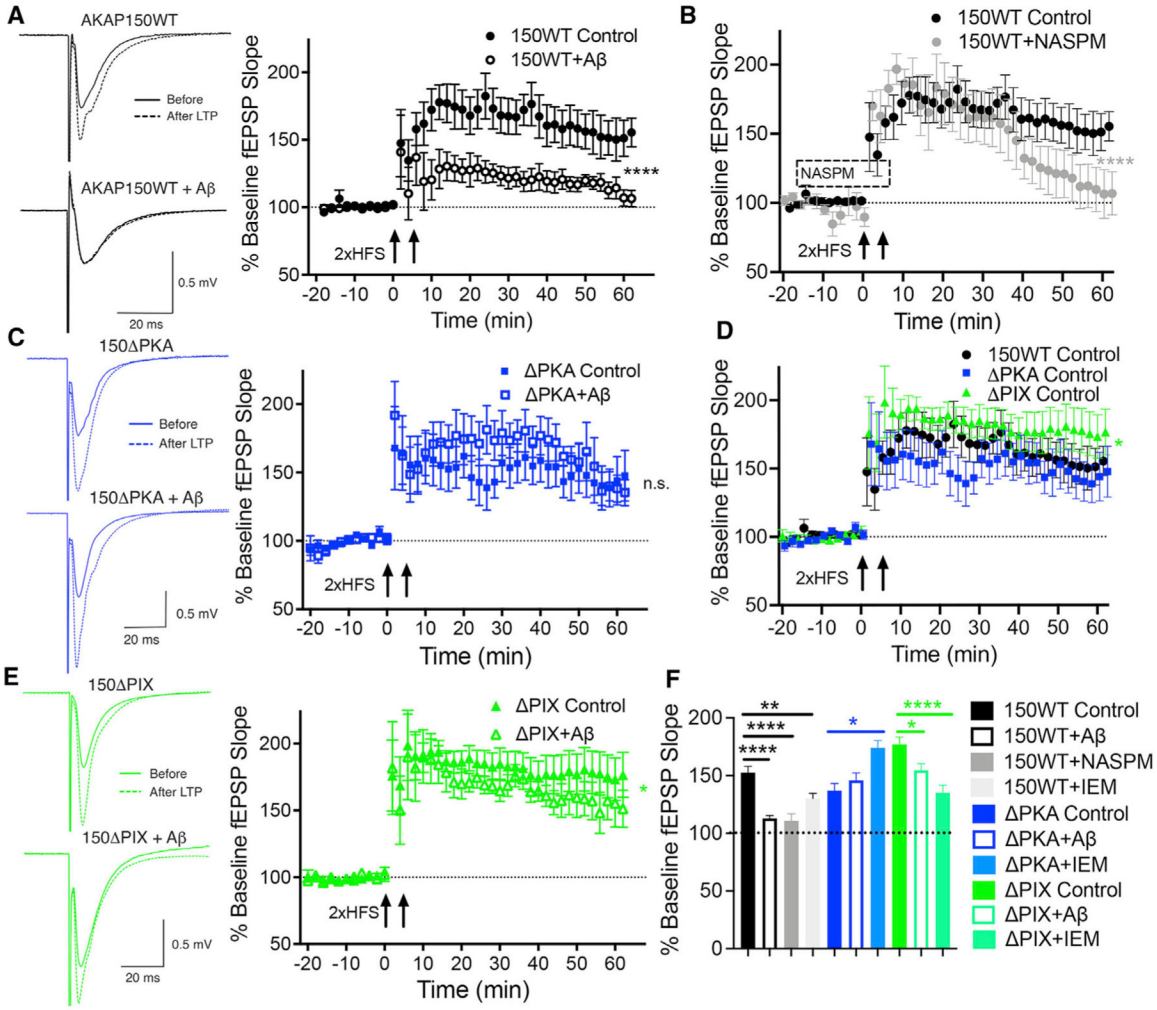

Figure 6. AKAP150-PKA and CaN anchoring are required for Aβ-mediated inhibition of LTP at SC-CA1 synapses in adult mice

(A and B) fEPSP recordings showing that LTP induced by spaced 2 × HFS is inhibited in the continuous presence of Aβ (control n = 6, Aβ n = 6, ****p < 0.0001 by 2-way ANOVA) (A) and by acute antagonism of CP-AMPARs (NASPM n = 5, ****p < 0.0001 by 2-way ANOVA) (B).

(C) LTP induced by spaced 2 × HFS in 150ΔPKA mice is insensitive to Aβ inhibition (control n = 7, Aβ n = 6).

(D) LTP induced by spaced 2 × HFS is of similar magnitude in WT, 150ΔPKA, and 150ΔPIX mice under control conditions (WT n = 6, 150ΔPKA n = 7, 150ΔPIX n = 10, *p < 0.05 to WT by 2-way ANOVA).

(E) LTP induced by spaced 2 × HFS in 150ΔPIX mice is largely insensitive to Aβ inhibition (control n = 10, Aβ n = 8, *p < 0.05 by 2-way ANOVA). (A, C, and E) Representative fEPSP recordings (left) and graphs of fEPSP slope normalized to baseline plotted over time (right) are provided.

(F) Normalized levels of fEPSP potentiation 52–62 min after LTP induction for the indicated conditions (WT control 153 ± 6, n = 36, WT+Aβ 113 ± 3, n = 37, WT+NASPM 111 ± 6, n = 30, WT+IEM 130 ± 5, n = 42; ****p < 0.0001, **p < 0.01 by one-way ANOVA

with Bonferroni's to WT control; ΔPIX control 177 ± 6, n = 60, ΔPIX+Aβ 155 ± 6, n = 48, ΔPIX+IEM 135 ± 7, n = 36; ****p < 0.0001, *p < 0.05 by one-way ANOVA with Bonferroni's to ΔPIX control; ΔPKA control 137 ± 6, n = 36, ΔPKA+Aβ 146 ± 6, n = 32; ΔPKA+IEM 174 ± 7, n = 36; *p < 0.05 by one-way ANOVA with Bonferroni's to ΔPKA control).

All data are represented as mean ± SEM.

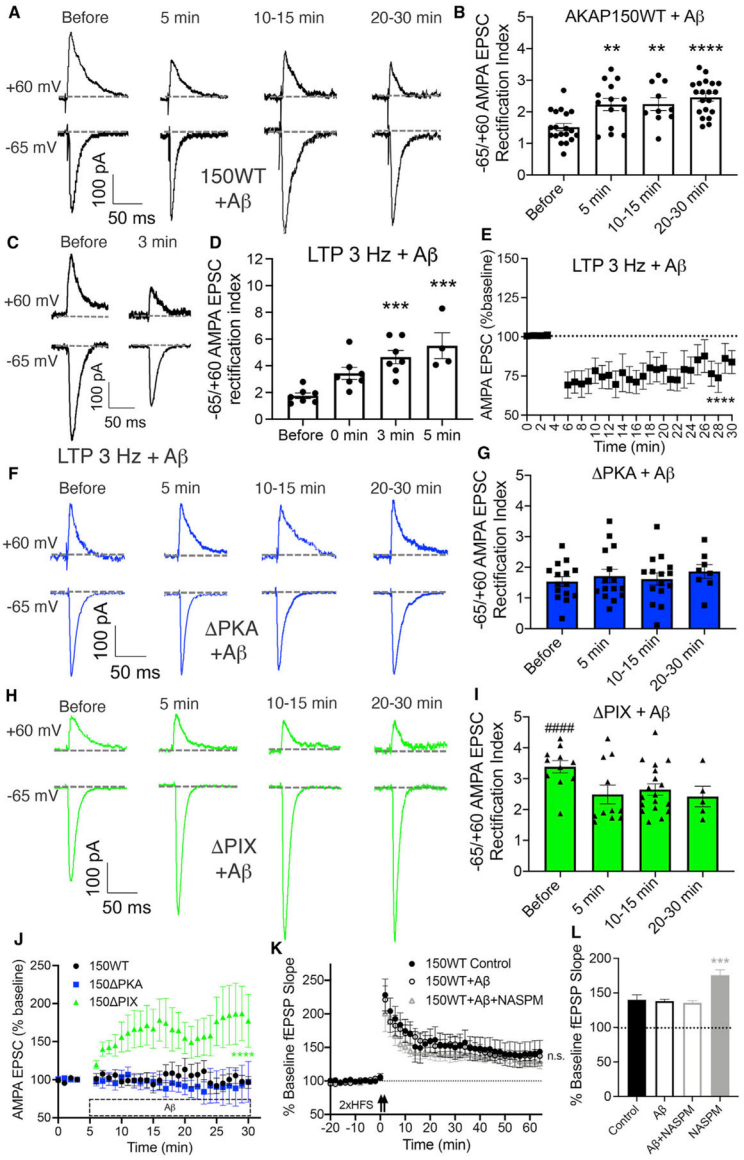

Figure 7. AKAP150-anchored PKA and CaN signaling oppose each other in regulating CP-AMPAR recruitment to SC-CA1 synapses, which primes Aβ-mediated LTP inhibition

(A and B) Representative traces (A) and graph (B) of the −65 mV/+60 mV AMPA EPSC rectification index, showing that extracellular of Aβ (100 nM) rapidly increases AMPAR rectification from 5–30 min after application in WT mice (Before n = 19; 5 min n = 14, **p < 0.01; 5–10 min n = 10, **p < 0.01; 20–30 min n = 20, ****p < 0.0001 to Before by one-way ANOVA with Dunnett's).

(C–E) Representative traces (C) and graph (D) of the −65 mV/+60 mV AMPA EPSC rectification index, showing that AMPAR rectification increases rapidly in WT mice 0–5 min after stimulation with an LTP induction pairing protocol (3 Hz, 0 mV, picrotoxin) in the presence of Aβ (100 nM) (Before n = 7, 0 min n = 7, 3 min n = 7, 5 min n = 4; ***p < 0.001 to Before by one-way ANOVA with Dunnett's) but results inappropriately in LTD (****p < 0.00010–3 min compared with=27–30 min, n = 8 by 2-way ANOVA) (E).

(F and G) Representative traces (F) and graph (G) of the −65 mV/+60 mV AMPA EPSC rectification index, showing that Aβ does not increase AMPAR rectification from 5–30 min after application in 150ΔPKA mice (Before n = 15, 5 min n = 15, 5–10 min n = 15, 20–30 min n = 10).

(H and I) Representative traces (H) and graph (I) of the −65 mV/+60 mV AMPA EPSC rectification index, showing that AMPAR rectification is increased basally in 150ΔPIX mice (Before n = 11, ####p < 0.0001 to WT Before in B by one-way ANOVA with Dunnett's) and that Aβ does not further increase AMPAR rectification (5 min n = 11, 5–10 min n = 18, 20–30 min n = 5).

(J) Aβ induces rapid potentiation of −65 mV AMPA EPSCs in 150ΔPIX mice (n = 9–12; ****p < 0.0001 compared with the WT by 2-way ANOVA) but not WT (n = 6–9) or 150ΔPKA mice (n = 7–10).

(K and L) fEPSP recordings (K) and normalized levels of fEPSP potentiation (L) 52–62 min after LTP induction, showing that LTP induced by massed 2 × HFS in WT mice is not inhibited by continuous Aβ exposure or by acute antagonism of CP-AMPARs (control 140 ± 7, n = 66; Aβ 138 ± 3, n = 48; Aβ+NASPM 136 ± 3, n = 48; NASPM 175 ± 8, n = 488, ***p < 0.001 increased compared with control by one-way ANOVA with Dunnett's).

All data are represented as mean ± SEM.

KEY RESOURCES TABLE

REAGENT or RESOURCE	SOURCE	IDENTIFIER
Chemicals, peptides, and recombinant proteins		
Tetrodotoxin (TTX)	Tocris Bioscience	Cat# 1078
Picrotoxin	Tocris Bioscience	Cat# 1128
QX-314 bromide	Tocris Bioscience	Cat# 1014
NASPM trihydrochloride	Tocris Bioscience	Cat# 2766
IEM 1460	Tocris Bioscience	Cat# 1636
DL-APV (AP5)	Tocris Bioscience	Cat# 0105
MK801	Tocris Bioscience	Cat# 0924
Spermine tetrachloride	Tocris Bioscience	Cat# 0958
Aβ (1–42) sodium salt, human	Anaspec	Cat# AS-6088
Experimental models: Organisms/strains		
AKAP150ΔPKA (allele symbol: $Akap5^{tm2Mdaq}$/$Akap5^{tm2Mdaq}$; Allele synonyms: Akap5ΔPKA, AKAP5ΔPKA)	Murphy et al., 2014	RRID: MGI_5702316
AKAP150ΔPIX allele symbol: $Akap5^{tm1Mdaq}$/$Akap5^{tm1Mdaq}$; Allele synonyms: Akap5ΔPIX, AKAP5ΔPIX)	Sanderson et al., 2012	RRID: MGI_5702308
C57BL/6J mice	Jackson Laboratories	RRID: IMSR_JAX:000664
Software and algorithms		
Prism	GraphPad	https://www.graphpad.com/scientific-software/prism/
pClamp/Clampfit	Molecular Devices	https://www.moleculardevices.com/
WinLTP	WinLTP Ltd. and The University of Bristol	https://www.winltp.com/
Mini Analysis	Synaptosoft, Inc.	http://www.synaptosoft.com/MiniAnalysis/